Wellesley College
Wellesley College Digital Scholarship and Archive

Honors Thesis Collection

2019

Evolutionary Development of the Mammalian Pre-Sternum

Zeynep Yozgyur
zyozgyur@wellesley.edu

Follow this and additional works at: https://repository.wellesley.edu/thesiscollection

Recommended Citation
Yozgyur, Zeynep, "Evolutionary Development of the Mammalian Pre-Sternum" (2019). *Honors Thesis Collection*. 670.
https://repository.wellesley.edu/thesiscollection/670

This Dissertation/Thesis is brought to you for free and open access by Wellesley College Digital Scholarship and Archive. It has been accepted for inclusion in Honors Thesis Collection by an authorized administrator of Wellesley College Digital Scholarship and Archive. For more information, please contact ir@wellesley.edu.

Evolutionary Development of the Mammalian Presternum

Zeynep Metin Yozgyur

Submitted in Partial Fulfillment
of the
Prerequisite for Honors
in Biological Sciences
under the advisement of Emily Buchholtz

April 2019

This material is copyrighted by Zeynep Yozgyur and Emily Buchholtz, April 25, 2019.

© 2019 Zeynep Yozgyur

Abstract

The mammalian sternum has undergone a reduction in relative size and complexity over evolutionary time. This transformation was highly variable across species, generating multiple, controversial interpretations. Some authors claim that the evolutionary reduction led to loss of presternal elements, while others believe that all, or some, presternal elements were fused into a structure ambiguously referred to as the “manubrium”, a term adopted from the post-interclavicular unit of pre-mammalian ancestors. Previous work on the *Paramylodon harlani* presternum revealed a composite presternum and identified three elements - mediocranial, mediocaudal and lateral - each with a different developmental origin and marginal articulation. This project used medical and micro CT scans to determine if these elements are conserved across species and if there is a characteristic histology associated with each. All three elements were identified in humans based on their locations and articulations. Their fusion during ontogeny was documented. Elements could not be associated with a characteristic histology. Instead, histology appears to reflect the mechanical forces to which different regions of the presternum are subjected, whatever their developmental origin. This opens the possibility that the presternum can be used to infer the limb use and locomotor style of extinct taxa. These lines of evidence indicate that the reduction of relative sternal size seen over evolutionary time has not led to element loss. Instead, three conserved elements with unique developmental origins and articulations are present in a composite presternum. Further, this reasoning suggests that the use of the term “manubrium” should be abandoned as ambiguous and instead when referring to specific areas on the presternum the terms interclavicle, sternal bands, and lateral elements should be used.

Contents

1. Introduction

The mammalian sternum is a highly variable and poorly understood anatomical unit in the thoracic ventral midline. Its differential classification as either axial or appendicular, and the disparate theories of its evolutionary transformation, are signals of its controversial interpretation. What is clear is that over mammalian evolutionary history the sternum as a whole has been reduced in relative size, and that the presternal subunit of the sternum has been reduced in element count. This project examines the hypothesis that the evolutionary reduction in presternal element count is primarily the result of the fusion of three ancestral elements, each with a discrete developmental origin and an articulation to a dedicated lateral structure. If supported, it suggests that evolutionary retention of presternal elements may reflect their unique developmental interactions. The project also tests the hypothesis that presternal elements are histologically differentiated, allowing reconstruction of an element's extent even after ontogenetic fusion. The project integrates classical and tomographic anatomical descriptions with the theory of mesodermal pattern domains recently embraced by developmental biologists. Because authors have assigned many different names to sternal, and especially presternal, structures, the default terminology below is adopted for this project, as demonstrated on the human skeleton (Fig. 1).

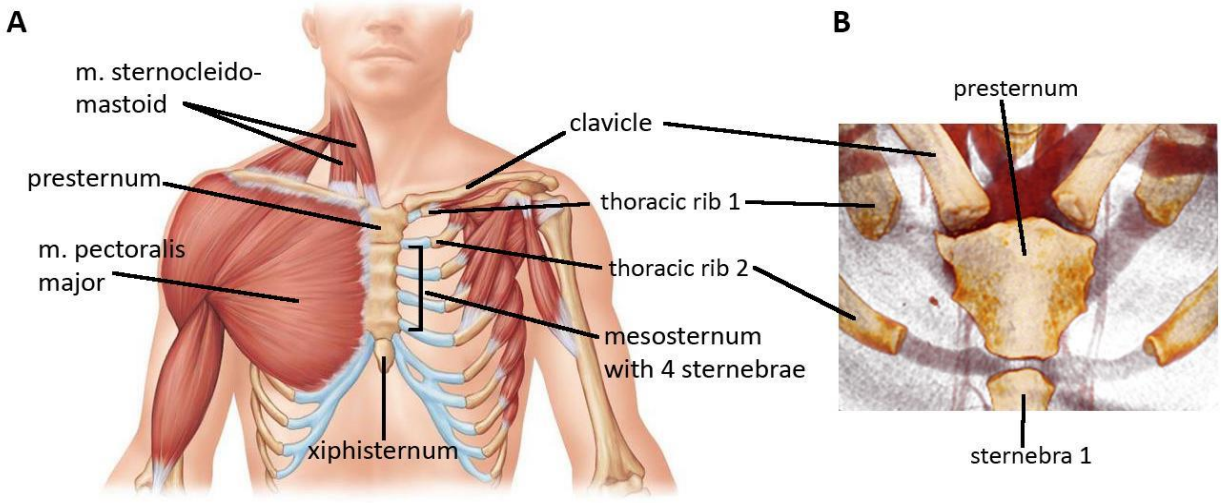

Figure 1. Sternal anatomy. A, generalized musculoskeletal anatomy of the human sternum, modified from https://tinycards.duolingo.com. B, Presternal structure and lateral articulating elements of Weaver Collection specimen W136, a 24.29-year-old male.

1.1. Sternal anatomy in major mammalian groups. Most taxonomic identifications of fossils occur on the basis of cranial and dental elements, and less often on postcranial elements (Gaetano et al., 2018). Based on the structure of the skull, three major groups of amniotes found in the Paleozoic Era have been identified: synapsid, anapsid, and diapsid. These groups are differentiated on the basis of temporal openings of the skull. The synapsid group, which has a single temporal opening, includes the early non-mammalian basal synapsids -- dicynodonts and cynodonts, as well as the living crown mammals – monotremes, marsupials, and eutherians (Fig. 2) (Angielczyk, 2009).

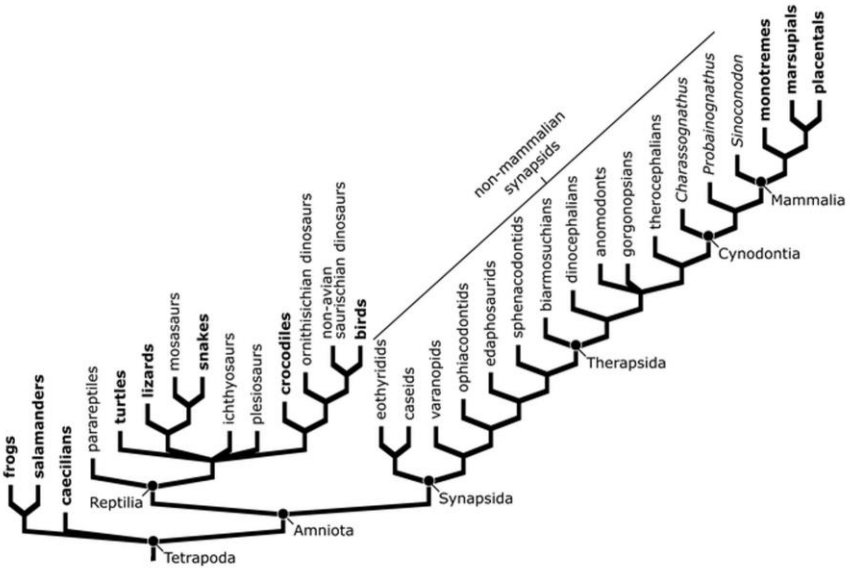

Figure 2. Simplified phylogeny of synapsid reptiles and their mammalian descendants. Modified from Angielczyk 2009 (Fig. 4B, p. 261).

The fossil record of mammals shows evidence of major reorganizations in the musculoskeletal system of the ventral shoulder girdle (Sereno, 2006). Fossil records of synapsid sterna are rare, but those that exist show an evolutionary sequence of an ancestral sternum that was restricted to the interclavicle in basal synapsids with a sprawling gait, an 'intermediate' sternum with an interclavicle that contacts a unit referred to as the "manubrium" and sternal bands in fossil cynodonts and living monotremes, and a sternum with reduced size and number of elements in placentals, suggesting adoption of parasagittal locomotion (Sereno, 2006).

Sternal elements are known for the early sphenacodontid synapsid *Dimetrodon* (Romer, 1956; Angielczyk, 2009) and for the cynodont *Diademodon* (Gaetano et al., 2018). The *Dimetrodon* sternum (Fig. 3) consists of a single, presternal element, the interclavicle. Its wide anterior end is slightly concave, and its posterior end is long, narrow and flat. It was identified as an interclavicle due to its surfaces for articulation with the large clavicles on its anterior end. Laterally it articulates with the scapula and coracoid elements of the dorsal shoulder girdle. The other presternal elements present in living mammals - the "manubrium" and the sternal bands - are not present, and there is no connection between the presternum and the rib cage.

The sternal elements of the cynodont *Diademodon*, known from a nearly complete specimen, were described by Gaetano et al. (2018). The left clavicle is convex and still attached to the interclavicle (Fig. 4). The interclavicle is preserved in its full form. In contrast to *Dimetrodon*, another presternal element is present: a "manubrium" separated into left and right halves. The left half is medially displaced; on its lateral side there is a projection of bone which is interpreted by Gaetano et al. (2018) as the proximal end of the first sternal cartilage. There is no visible suture between the thoracic rib and the "manubrium." The second rib is fused with

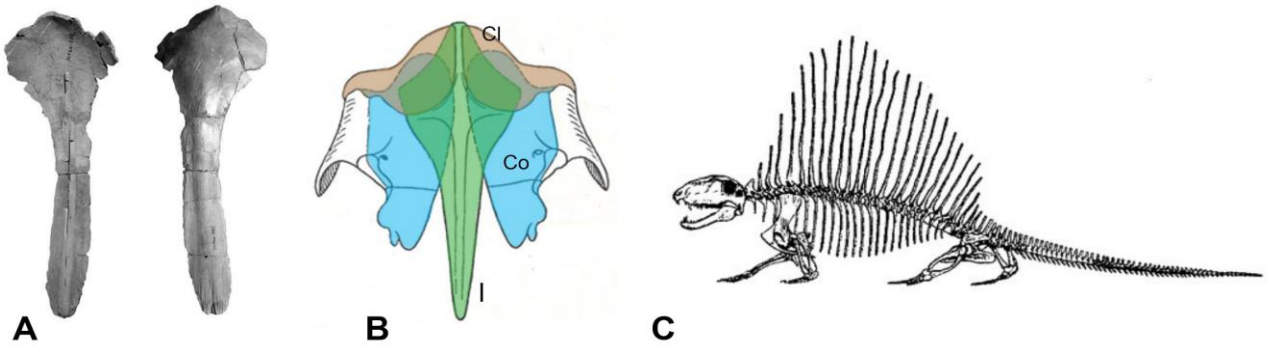

Figure 3. Sternal anatomy in *Dimetrodon*. A, dorsal and ventral views of the interclavicle of *D. gagashomogenus* from Hunt and Lucas (2005). B, schematic of the interclavicle and the articulating clavicle (Cl) and coracoid (Co), modified from Romer (1956). C, skeletal reconstruction of *Dimetrodon* from Romer (1927).

and positioned posteriorly to the preseternum. The right half of the "manubrium" is not in its natural position, but rather rotated to the right. The fact that there are two presternal elements that are separated indicates that these halves were originally bilaterally paired. As will be described below, this trait is characteristic of sternal bands, which originate as two unsegmented paired elements.

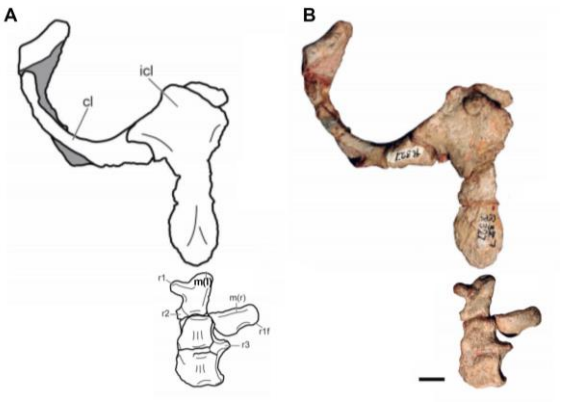

Figure 4. Sternal anatomy of *Diademodon* in dorsal view, modified from Gaetano et al. (2018). A, diagram of bone elements. B, fossil in dorsal view. cl = clavicle; icl = interclavicle; m(l) = left "manubrium", m(r) = right "manubrium"; r1, r2 = thoracic ribs 1, 2, etc.; r1f = rib 1 facet. Scale bar = 10mm.

The sterna of living monotremes closely resemble that of the cynodont *Diademodon* in that they possess a large interclavicle, a discrete "manubrium," and a string of sternebrae that articulate with the thoracic ribs (Fig. 5). Monotreme sternal anatomy and development have been described by Parker (1868), Griffiths (1978), and Klima (1973). The lateral parts of the T-shaped interclavicle are composed of membranous bone and articulate with the clavicles (Griffiths, 1978). As in cynodonts, the presternum is clearly separated into elements, each having a unique articulation: the interclavicle articulates with the clavicle, the "manubrium" with the first thoracic rib, and the sternal bands with the second and subsequent ribs.

Most placental mammals (marsupials and eutherians) have a segmented sternum with all three major units: presternum, mesosternum and xiphisternum. The interclavicle is no longer

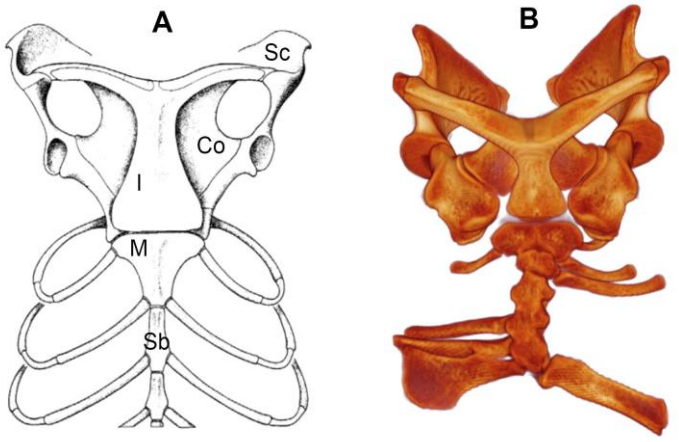

Figure 5. Sterna of living Monotremata. A, *Ornithorhynchus anatinus* (platypus) after Klima, 1973 (Fig. 1, p.11); B, *Tachyglossus* sp. (echidna), reconstructed from CT data provided by Z. Luo. Co = coracoid; I = interclavicle; M = "manubrium"; Sb = sternal bands; Sc = scapula.

identifiable. Instead, a single element, the presternum, articulates with all three lateral articulating structures (Fig. 6). Anteriorly the presternum articulates with the clavicle, laterally it articulates with the first thoracic rib, and posteriorly it articulates with the second rib, which is positioned between the presternum and the first pair of sternebrae. The presternum has a trapezoid-like shape, being wider at its articulation with the first rib. It narrows and is elongated posteriorly. The second sternal rib attaches between the presternum and the first mesosternal sternebrae (Fig. 6C) (Parker, 1868).

Both marsupial and eutherian sterna are remarkably plastic in morphology, as documented by multiple comparative anatomists and most notably in the monograph by Parker (1868). Most species exhibit all three units of the sternum, but they can be variably expressed (Fig. 6A, C). For example, the presternum is greatly expanded in the marsupial mole (Fig. 6C), which has hypertrophied first ribs. In contrast, both the mesosternum and the xiphisternum can be absent when there are no sternal ribs, as in mysticete whales (Fig. 6D).

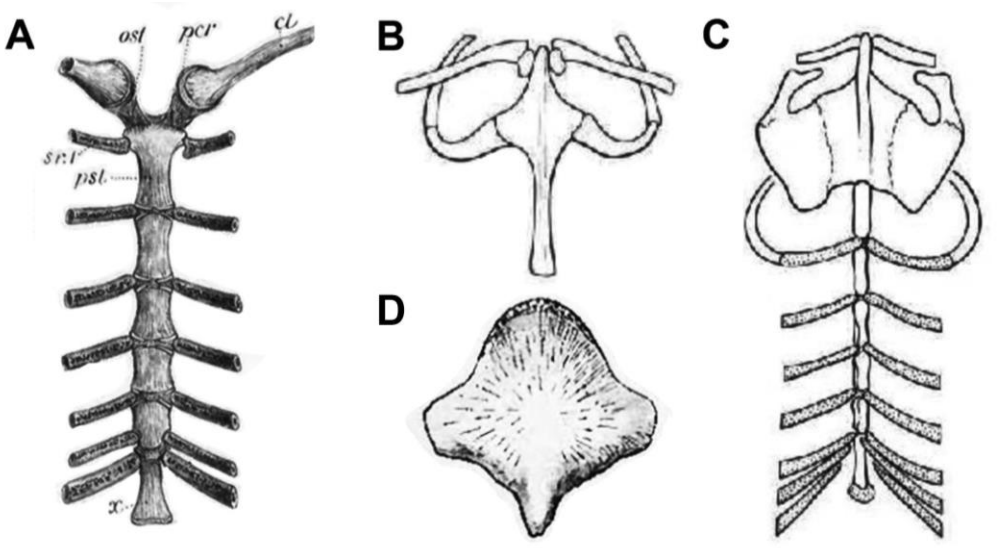

Figure 6. Sterna of living marsupial and eutherian placental mammals. A, the placental *Lepus canniculus* (European rabbit) after Parker (1868); B, the marsupial *Lestoros inca* (Incan shrew

mole) after Klima (1987); C, *Notoryctes typhlops*, the marsupial mole, after Klima (1987); D, the placental baleen whale *Megaptera* sp. after Struthers (1889).

1.2. Overview of the developmental biology of the mammalian sternum. The vertebrate musculoskeletal system originates from the mesodermal germ layer. This system is classically divided into axial and appendicular musculoskeletal components. The axial skeleton includes the vertebrae, the vertebral ribs, the sternum and the attached musculature. The appendicular skeleton includes the bones of the limbs, the associated girdles and the attached muscles. The largest muscle groups that have origin or insertion on the sternum include muscles of the forelimb (e.g. pectoralis major) and of the head and neck (e.g. sternohyoid, sternothyroid, sternomastoid) (see Fig. 1). Additionally, the diaphragm attaches to the xiphisternum. (https://opentextbc.ca/anatomyandphysiology/).

Two different mesodermal cell populations - the somitic mesoderm and the lateral plate mesoderm - contribute to these musculoskeletal elements. These embryonic populations develop in very distinct environments, termed the primaxial and abaxial domains (Burke and Nowicki, 2003). They are separated by a developmental boundary, termed the lateral somitic frontier. All skeletal muscles originate from somitic cells in the primaxial domain. Some myoblasts remain and differentiate in the primaxial domain, and this includes muscles directly associated with the axial skeleton and vertebrae. In contrast, the limb bud forms from the lateral plate mesoderm, in the abaxial domain. Some myoblasts migrate from the primaxial domain into the limb bud and differentiate in the environment of the lateral plate mesoderm. These myoblasts become musculoskeletal tissues of the appendicular skeleton and are also considered abaxial. The sternum, part of the axial skeleton and thoracic cavity, has its origin in the lateral plate mesoderm, and is thus considered abaxial. That is unusual as all other axial skeletal elements belong to the primaxial domain (Fig.7) (Burke and Nowicki, 2003; Durland et al., 2008). The interaction of the abaxial sternum with the primaxial ribs across the lateral somitic frontier is thus of particular interest. This interaction has an analog in the pelvis, which is also abaxial and also interacts directly with the primaxial vertebral column (Griffin and Angielczyk, 2019).

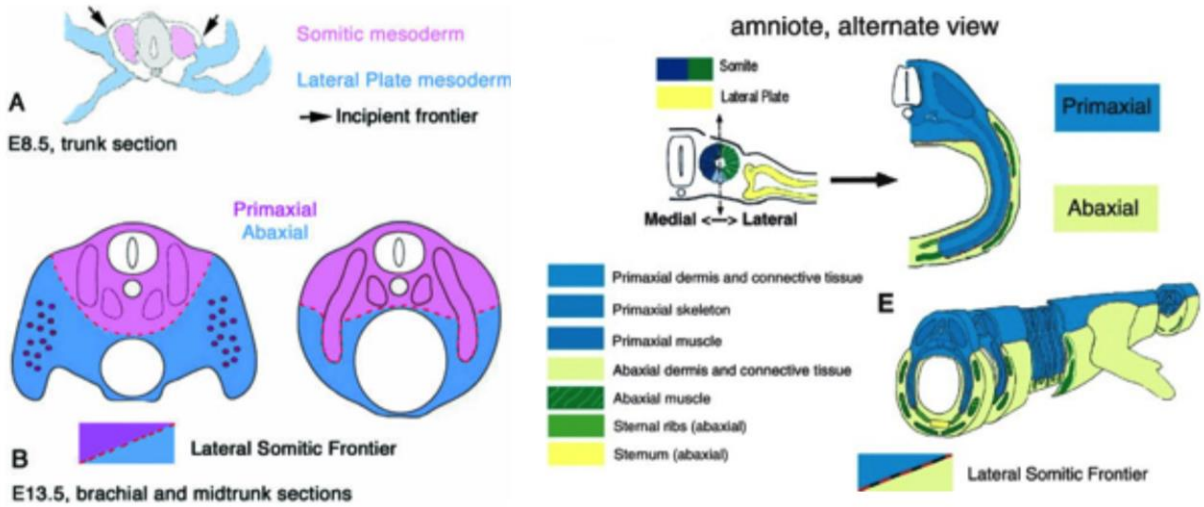

Figure 7. Schematic representation of an embryo showing the primaxial and abaxial domains and the lateral somitic frontier. After Durland et al., 2008 (Fig. 1 A, B) and Burke and Nowicki, 2003 (Fig. 1 E).

The skeletal classification of the sternum is ambiguous. Anatomically, it belongs to the axial skeleton, i.e. the central axis of the skeletal system, which is the meeting point of the ribs. Functionally, it supports the muscles of the pectoral girdle - sternocleidomastoid, sternohyoid, sternothyroid, and pectoralis major, and might therefore be considered appendicular. The pectoral girdle, which includes the clavicle and scapula, belongs to the appendicular skeleton.

Developmentally, the *Tbx5* gene regulates the formation of the limbs and the pectoral girdle as well as the sternum. Expression of *Tbx5* gene occurs in two regions of the forelimb - 1) the superficial tissues of the thorax, where axioappendicular muscles attach the appendicular limb to the axial body, and 2) the ventral midline region of the thorax, where the sternum develops. *Tbx 5,* expressed in the lateral plate mesoderm, is necessary not only for appendicular forelimb formation, but also for formation of the girdle structures (scapula, clavicle and sternum) and the girdle muscles that have points of insertion on the axial skeleton (Valasek et al., 2011).

1.3. Detailed development of major sternal units. The development of the mesosternum from the sternal bands is well-established and is treated first here. Contrary to classic theories (Ruge, 1880), the sternal bands are not derived from the ribs (Chen, 1952), although older individuals with an ossified rib cartilage often show an intimate contact between the ribs and the sternum. Rather, sternal bands form from mesenchymal condensation of lateral plate mesoderm near the limb bud. Closure of the sternal bands, i.e. the fusion of the left and right bands in the ventral midline, was previously thought to be due to the elongation of the ribs, which were suggested to provide either a chemical or a mechanical signal. An *in vitro* experiment in mice by Chen (1952) demonstrated that the complete removal of the ribs still allowed for a complete fusion of the sternal bands. However, the absence of ribs did impact the segmentation of the sternal bands - there was none. Chen demonstrated (1952) that each rib stump, and no other skeletal element, has a hypertrophy-inhibiting effect on the half of the sternal band that it contacts. Sternebrae halves with no rib stump result in a decrease in the inhibitory effect and an increase in hypertrophy of the cartilage cells throughout the length of the sternum (Chen, 1952). This inhibitory effect occurs at the lateral somitic frontier, where primaxial and abaxial domains interact. Ribs and the sternum thus have different mesodermal origins and exhibit inhibitory interaction where they interact.

The presternum, also derived from lateral plate mesoderm, condenses in place. Using sectioned and stained specimens, Rodriguez-Vasquez (2013) identified early formation of an anterior midline mesenchyme in human embryos (Fig. 8). As early as week 6, a mesenchymal condensation appeared continuous with the clavicles, but separate from both rib 1 and the sternal bands. Rodriguez-Vazquez (2013) called that region the “interclavicular mesenchyme”. Initially, the sternothyroid and sternohyoid muscles were positioned adjacent to the interclavicular mesenchyme and the the sternal bands were attached to the pectoralis major muscle. Later, the interclavicular mesenchyme joined the anterior end of the first ribs via an

"intercostoclavicular mesenchyme." This did not affect the fusion of the sternal bands positioned posteriorly. The sternal bands still kept a close attachment to the pectoral muscles. At a later stage, the sternoclavicular ligament and the interclavicular ligament separate the presternum from the clavicle and first ribs. These findings of an existing interclavicular mesenchymal condensation are similar to the predictions of Muller and O'Rahilly (1986), who proposed the existence of an "interclavicular blastema" that joins the sternal bands, and of Keibel and Mall (1912) who proposed the existence of an episternum, a structure already joined to the sternal bands and to the anlage of the clavicle.

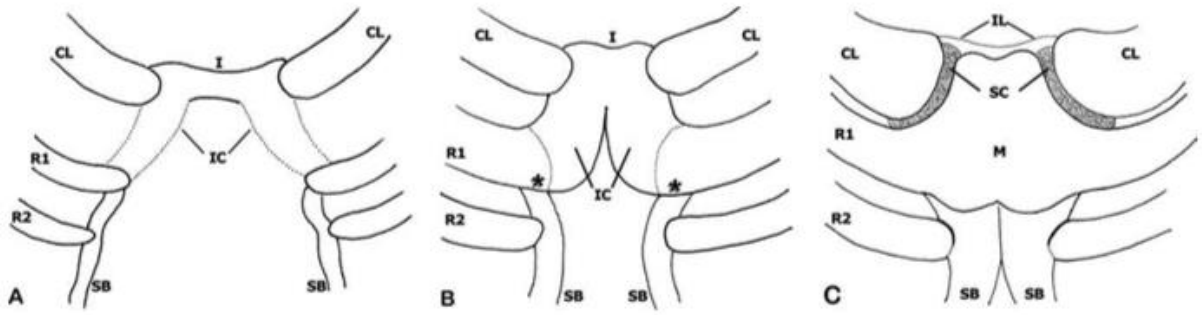

Figure 8. Stages of "manubrium" formation in human embryos, as described by Rodriguez-Vasquez (2013). A, B, and C are sequential stages. CL = clavicle; I = interclavicular mesenchyme; IC = intercostoclavicular mesenchyme; IL = interclavicular ligament; M = "manubrium"; R2, 2 = rib 1, 2, etc.; SB = sternal bands; SC = sternocostoclavicular joint.

In a ground-breaking study of the rib cage, Durland et al. (2008) showed that the thoracic region of mice is made of seven 'true' ribs that connect to the sternum and six 'false' ribs which do not reach the sternum. Additionally, labelling of thoracic periosteum showed that the relationship of the first thoracic rib to the presternum is different from that of the subsequent ribs to the sternal bands. Labelling of the periosteum of the first rib showed that the first rib joint and sternum join in an abaxial : abaxial fusion. Therefore, the periosteum of the first rib (and only the first rib) is patterned along with the lateral plate mesoderm (Durland et al., 2008). Additionally, the first rib of humans is different in its ossification pattern compared to the subsequent ribs. Ossification of the first rib begins in the early 20s, with a formation of osseous islands and precedes ossification of the other costosternal ribs, which do not begin to ossify until the age of 50. Its direct fusion (synostosis) with the presternum contrasts to the other ribs, which articulate moveably with the sternum. These observations confirm that the relationship of the first rib to the presternum is different than that of the other costosternal ribs to the sternal bands, both morphologically and developmentally (Barchilon et al., 1996; Durland et al., 2008).

1.4. Bone Remodeling. On a morphological level, the external architecture of a bone provides functional information based on its muscle attachments and articulations with other bones. On a histological level, bone can be differentiated into a compact outer cortical layer and a spongy, or cancellous, trabecular inner layer. Cancellous bone is the major type of bone tissue found in the appendicular skeleton and thus is considered the main load-bearing bone in the body. Cancellous bone is characterized by trabecular tissue which is highly porous, filled with bone

marrow and blood vessels, and has a high elasticity. The airy nature of the bone allows it to have an increased surface area and a better use of calcium resources which contributes to the especially high rate of remodeling and metabolic activity (Oftadeh et al., 2015). The proportion of cortical to spongy bone and its internal structure can give functional information about the location of articulating structures and behavioral information about the bone's response to mechanical stress. The skeletal system, and more so trabecular bone, is highly malleable, adaptive and responsive to change caused by mechanical stress (Oftadeh et al., 2015).

Trabecular orientation is dependent on the stress exerted in the environment. Trabeculae align themselves preferentially in the orientation of the loading stress during the dynamic remodeling process. Most commonly trabecular structure is quantified by measuring degree of anisotropy, which shows the preferred orientation of trabeculae in a 3D space, and the proportion of trabecular to total bone volume, which measures the porosity of the bone (Kivell, 2016). Bone remodeling is dependent on both the load of the mechanical stimuli and the period of duration of the stimuli. Dynamic external loading can have a dramatic effect on anisotropy as well as volume ratio. Bone adaptation is also highly localized due to the strain acting locally between bone articulations or muscle insertions (Kivell, 2016). Kivell (2016) documented adaptations in trabecular volume ratios and in the alignment of trabeculae in response to the direction of the stressor. Analysis of the trabecular structure of the human sternum by Arbabi (2009) showed that the presternal units have more and longer trabeculae, a higher percentage of bone, and less bone marrow space than the mesosternum. This means that the presternum is more able to resist stress, both pressure and tension, than the mesosternum, and is adaptable to change (Arbabi, 2009).

1.5. Theories of presternal evolution. Reduction of presternal elements as seen in placental mammals has been previously interpreted by three theories: 1) as a result of element loss, 2) as a result of element fusion, or 3) both. Previous theories on the evolutionary history of the mammalian sternum were proposed by Parker (1898), Klima (1973, 1985, 1987), and Luo (2007, 2011, 2015). Evolutionary transformation of the sternum is often hard to trace because of the limited numbers of fossils that have been found and pieced together, and because of the extremely small size of early eutherians.

Theories advocating an evolutionary reduction in presternal element count have been most strongly supported by Klima's work on marsupials and monotremes in the later half of the 20th century. According to Klima (1985), the interclavicle in monotremes (e.g. *Ornithorhynchus*) has two histological origins - a paired lateral element, consisting of membranous bone tissue (Fig.9, icd), and an unpaired medial element, consisting of cartilaginous tissue that is replaced by bone during development (Fig. 9, icc). The rest of the sternum is composed of paired sternal bands. In marsupials and placentals the ventral dermal unit (Fig.9, icd) is absent. The unpaired midline portion of the interclavicle exists in the embryonic state, but it later fuses with the unpaired sternal bands, forming the "manubrium" in the adult. There is therefore no recognizable interclavicle, and the clavicle articulates with the tip of the "manubrium" (Klima, 1973). The left and right half of the marsupial sternal bands are separate initially, and slowly begin to approach the midline during embryonic development. The interclavicle, which sits between the sternal

bands and the clavicle, is present in the marsupial embryo. However, Klima argues that this condensed mesenchymal element is actually a remnant of a more lateral element, the procoracoid (a shoulder-girdle component).

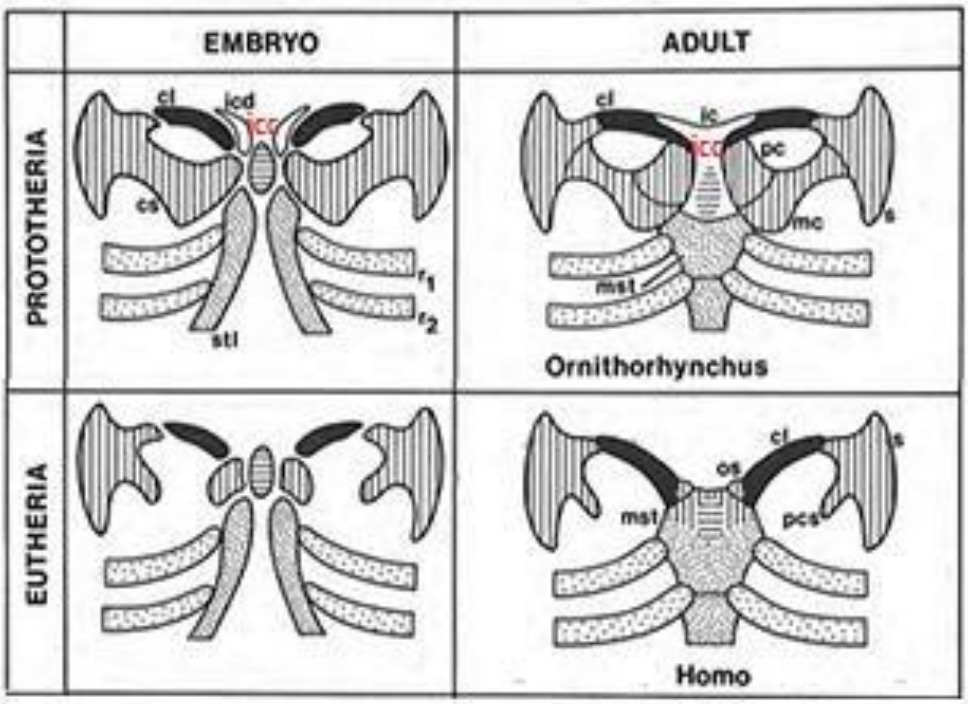

Figure 9. Comparison of the development of the shoulder girdle and sternum in prototherian (Monotrema), and eutherian mammals, modified from Klima (1985). cl = clavicle; cs = coracoid-scapular plate, ic = interclavicle; icc = unpaired midline portion of interclavicle; icd = paired dermal element of the interclavicle; mc = metacoracoid; mst = “manubrium” sterni; os = suprasternal ossicle; pc = procoracoid; pcl = praeclavium; pcs = coracoid process; r1,2, = rib1,2; stl = sternal band.

A variant of the reduction theory, i.e. a remodeling of the sternum by a fusion following a reduction in presternal elements, was suggested by Luo (2011). The common ancestor of stem therians and crown therians exhibited a large interclavicle, with a broad anterior region and an interclavicular lateral process, that comes in contact with the length of the clavicle (Fig. 10). The interclavicle joins the “manubrium” posteriorly, forming a synovial joint. In monotremes, the coracoid process on the scapula is massive; it reaches to and articulates with the joint formed between the interclavicle and the “manubrium,” posterior to it (Fig. 10). In addition, Luo defines embryological, developmental and topographic differences between the interclavicle and “manubrium,” which are recognizable in extinct monotremes. During embryogenesis, the interclavicle forms from membranous (lateral) and endochondral (medial) bone, whereas the “manubrium” is exclusively endochondral (Luo, 2011).Moreover, the “manubrium” develops from the sternal bands connected to the first thoracic rib and in general the “manubrium” is the only pre-sternal element which has a direct contact with the first rib, as the interclavicle does not (Luo, 2011). Compared to their common ancestors, in Luo’s interpretation, the triconodont

and the crown therians exhibited a loss of the procoracoid, a reduction in the length and shape of the interclavicle, and a loss of the interclavicular lateral process (Fig. 10). This loss of the procoracoid is interpreted as increasing the mobility of the shoulder girdle, as there is no articulation with the presternum, as in monotremes (Luo, 2011). Crown theria exhibit an even larger reduction in presternal elements. The embryonic interclavicle is proposed to incorporate into a single unit, identified as the "manubrium," with articulation to the clavicle, the first thoracic rib, and the second thoracic rib (Luo, 2011). Luo attributes this skeletogenesis to changes in cell condensations either due to proliferation or to differentiation, or to localized heterochrony. Genetic expression of the *Hox* genes in marsupials shows patterning zones along the anterior-posterior axis, which predicts an embryonic and/or ancestral structure of two units placed in anterior - posterior sequence (Luo, 2011; Keyte and Smith, 2010). This finding challenges the traditional terminology, as the "manubrium" is then used to label two different units within the same presternal structure.

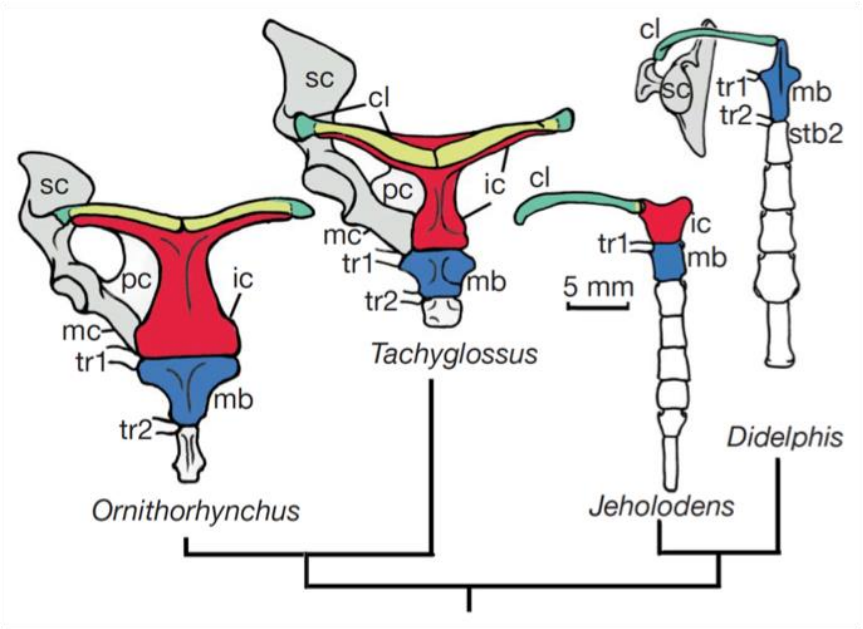

Figure 10. Transformation of the presternum from a multi-element to a single element structure, modified from the proposal by Luo (2015). cl = clavicle; ic = interclavicle; mc = metacoracoid; mb = "manubrium"; mc = metacoracoid; pc = precoracoid; sc = scapula; stb = sternebra; tr1, 2 = thoracic rib 1, 2.

Presterna of fossil ground sloths with surficial evidence of multiple components were first identified in the fall of 2016 at the La Brea Tar Pits Page Museum by Tim Gaudin, Greg McDonald, and Emily Buchholtz. Multiple specimens were photographed on site (Fig. 11) and four were later CT scanned at the Cummings School of Veterinary Medicine - Tufts University.

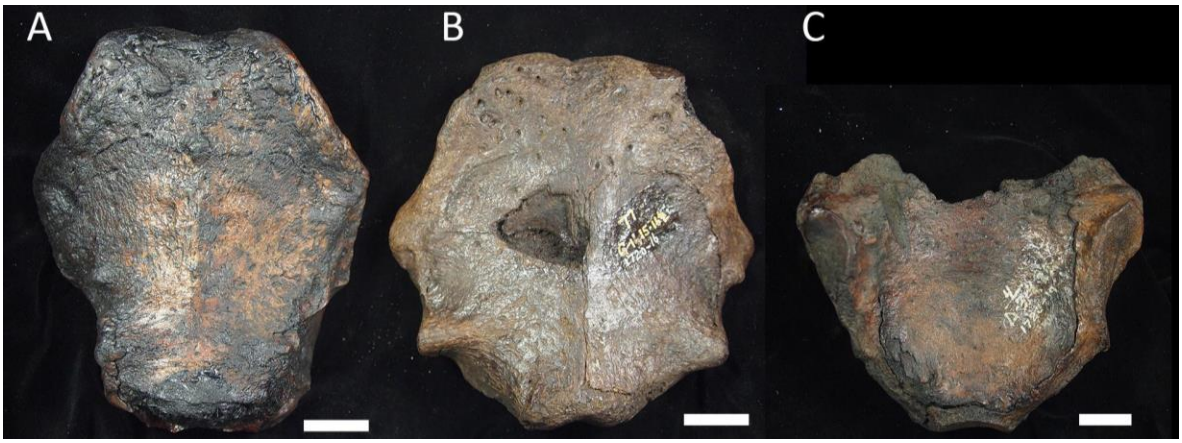

Figure 11. Ventral (A, B) and dorsal (C) views of *Paramylodon harlani* presterna from the collections of the La Brea Tar Pits Page Museum. A, HC 1720-13, ventral view; B, HC1720-16, ventral view; C, 1720-19, dorsal view. Note the presence in persternal seams and regional differences in bone texture. All scale bars = 2 cm.

Asher Feldman segmented some of these scans for a BISC 350 project in the spring of 2017. His work identified internal sutures delimiting presternal elements inconsistent with the predictions of both Klima and Luo (Fig. 12). In particular, it identified a bilateral suture in the presternum that lies in parasagittal plane lateral to the midline at the medial end of the first thoracic rib (Fig. 12), defining a previously unrecognized presternal subunit. This project is inspired by and continues Feldman's work using additional strategies across a wider range of taxa.

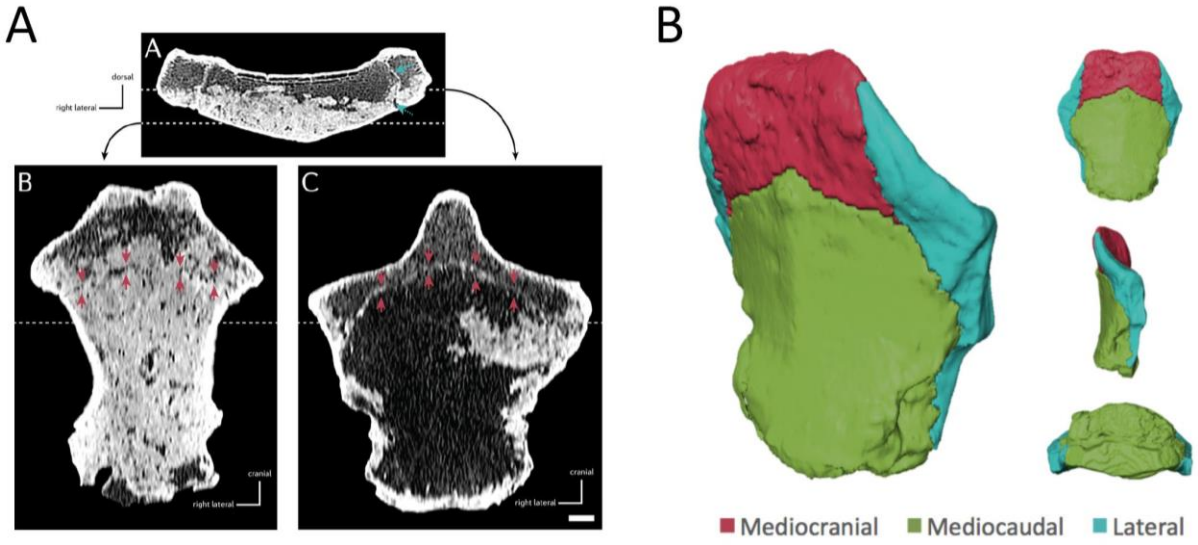

Figure 12. *Paramylodon harlani* presternum HC 1720-13, as imaged and segmented by Asher Feldman (2017). A, CT scan in three planes; B, segmented image colored to display regions demarcated by internal boundaries.

1.6. Homology. The theory of evolution proposed by Darwin (1859) recognized both the transformation of individual species (anagenesis) and the shared common ancestry of all species (cladogenesis). Recognition of shared ancestry must by definition be inferred and is therefore subject to interpretation. The keystone of any inference of common ancestry is the recognition of traits or structures in different species that have evolutionary descent from a shared ancestral trait or structure in the common ancestor. But the very fact of evolutionary transformation makes the recognition of these homologs challenging. Raff (1996) synthesized multiple theories of homology, defining homologous structures as those that "share a common evolutionary origin and an underlying commonality of morphology resulting from a continuity of information."

Methods for recognizing homologs precede Darwin and the theory of natural selection. Based on a theory of archetypes instead of evolution, Richard Owen (1846) recognized "similarity, position, and connections" as criteria for homology. These criteria have not changed radically over the last 170 years but are now understood as the product of shared evolutionary history. Reidl (1978) laid out positional, structural, and transitional criteria for the recognition of homologs. The positional criterion requires similarity of position in a comparable structural system, whether anatomical or molecular. The structural criterion uses similarity of morphological detail, even when a structure is displaced anatomically (e.g. testes or DNA base sequences). The transitional criterion relies on incremental stages between end members of a comparative set. These stages may occur either in ancestor / descendant series or in an ontogenetic (developmental) series. More recently, Wagner (1994) proposed similar criteria: phylogenetic continuity, structural identity, and shared developmental history. In this project, homology of individual elements of a complex structure (the presternum) will be inferred using positional, structural, and ontogenetic (developmental) criteria.

1.7. Variations of the human presternum. Bayarogullari et al. (2014) documented multiple ossification patterns of the presternum of humans that were interpreted as anomalies in individuals aged between 0 and 20 years-old. The authors did not include older individuals because ossification centers in the sternum fuse by 12 years of age. The existence of two to four ossification centers in individuals between 0 to 10 years of age was observed in 14% of their data. A greater number of ossification centers was observed in ages between 0 and 5 years with two individuals having four ossification centers, three having three ossification centers and eleven having two ossification centers. In the second age group - ages between 6 and 10 years, only one individual had four ossification centers, one had three ossification centers, and eight had two ossification centers. In the later age groups between 11 and 20 years, there were only two individuals with two ossification centers (Bayarogullari et al., 2014).

2. Materials and Methods

This project used two major databases - thoracic computed tomography (CT) scans of humans for the documentation of presternum element composition and micro CT scans of comparative species for the histological and functional analysis of the presternum.

2.1. Human CT scans. A database of 355 human thoracic CT scans was provided by Dr. Ashley Weaver from the Wake Forest University School of Medicine, NC. HIPPA privacy regulations required that individuals be stripped of all identifiers except age and sex. Scans of infants are unusual, and therefore it seems likely that the youngest individuals in the database may have had medical interventions for a variety of possible conditions such as heart surgery. The possible effects of these conditions on sternal anatomy are unknown.

Four scans were removed from the database: one duplicate, and three files unreadable due to either a medical intervention or because of inability to load the data into the visualization program. The remaining 351 scans consisted of 178 females and 173 males ranging from 0.01 to 97.32 years of age (Fig. 13). 165 scans were from individuals aged 0-9 years, and 186 scans were from individuals aged 10-99 years (Fig. 13). The scans from individuals over 10 years of age were distributed roughly equally, with 19 to 23 individuals within each 10-year age bin. Three of the individuals from the 0-9 age group had multiple scans over time: two scans from an individual at ages 1.49 and 3.44 years; four scans from a second individual at ages 0.3, 0.47, 1.28, and 1.87 years, and two scans from a third individual taken at ages 0.74 and 0.89 years.

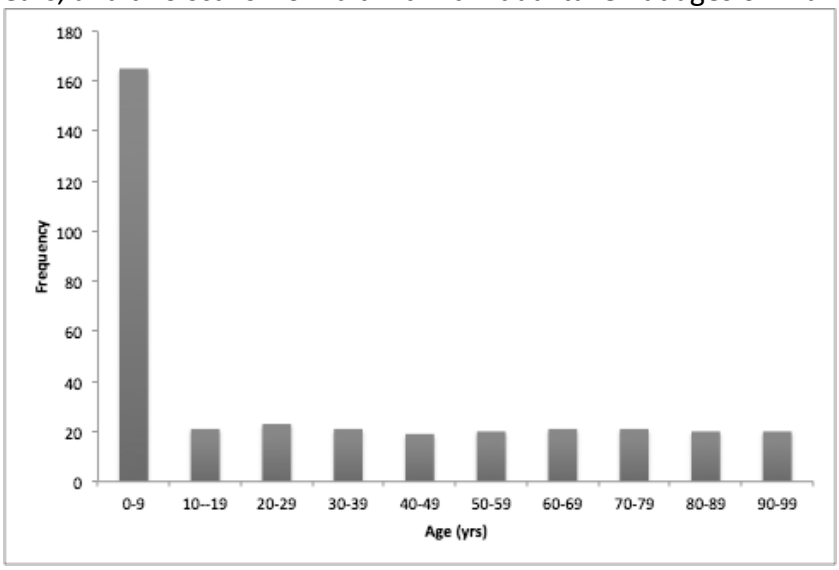

Figure 13. Age distribution of the individuals in the Weaver thoracic CT scan database. Each bar corresponds to a bin of 10 years of age.

The human thoracic CT scans were visualized using AMIRA Software - a 3D visualization and analysis software program (Version 5.4). Direct volume rendering was performed using the Volren function. Color and Transparency were edited for better rendering and enhancing detail. The VolrenGlow colormap was used for color, as it was considered to have a color pattern

closest-looking to the human skeleton. The VolumeEdit function was used to cut and edit the image in order to display the sternum, attached sternal cartilages, ribs and clavicle without being obscured by additional tissue and organs.

Reconstructed images were evaluated for the presence and location of component presternal elements. When multiple elements were present, location (anterior vs posterior), symmetry (paired bilateral vs unpaired medial), and the identity of articulating lateral structures (clavicle, thoracic rib 1, thoracic rib 2) were used to identify homologs. An example of element analysis is provided in Fig. 14. In this example, individuals A and B (left) are superficially similar: a large anterior midline unit is separated from multiple smaller posterior units. When additional tissue is removed to show sternal articulations (right), it is clear that thoracic rib 2 articulates posterior to the the large midline unit in A, but behind the second, smaller unit in B. The two most anterior units in B were therefore interpreted as the unfused homologs of the single first unit of individual A.

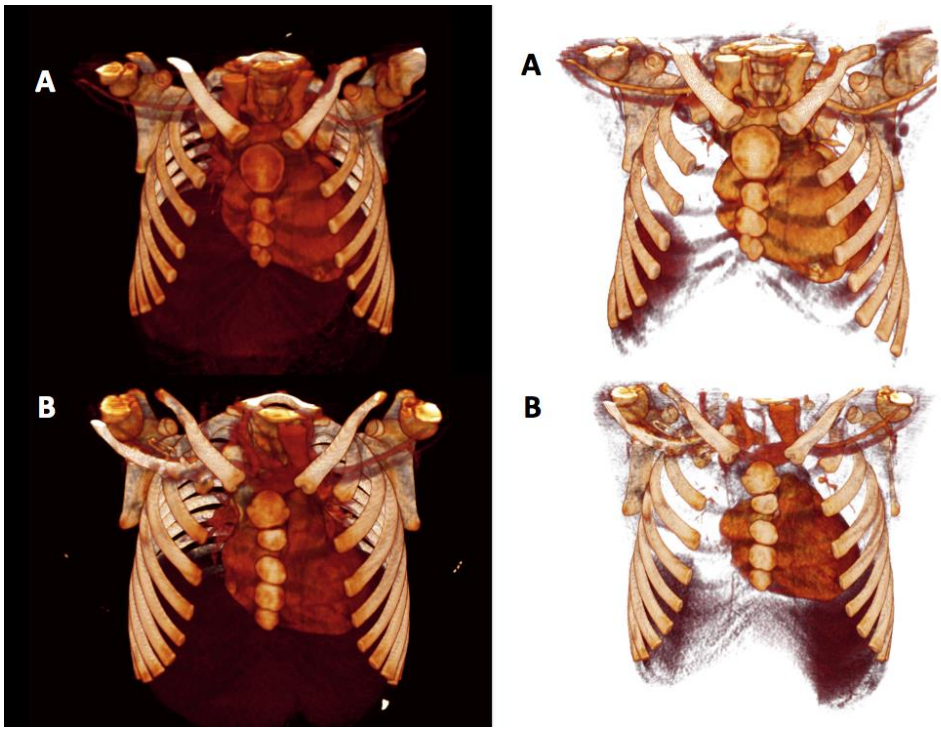

Figure 14. Visualization of sternal elements in two individuals before (left) and after (right) removal of blocking tissue. A, W656, aged 3.69 years; B, W662, aged 4.23 years.

Because the elements in human scans coincided in both location and structure with those identified in the fossil sloths by Feldman (2017), the same positional identities were used: the midline elements include an unpaired **mediocranial** element associated with the clavicle, and paired **mediocaudal** elements that articulate with thoracic rib 2 and with the first sternebrae. These midline elements separate the paired **lateral** elements, which articulate with thoracic rib 1. There is a maximum of five elements which allowed for the hypothesized construction of a variation of nine patterns of element organization (A - I) (Fig.15).

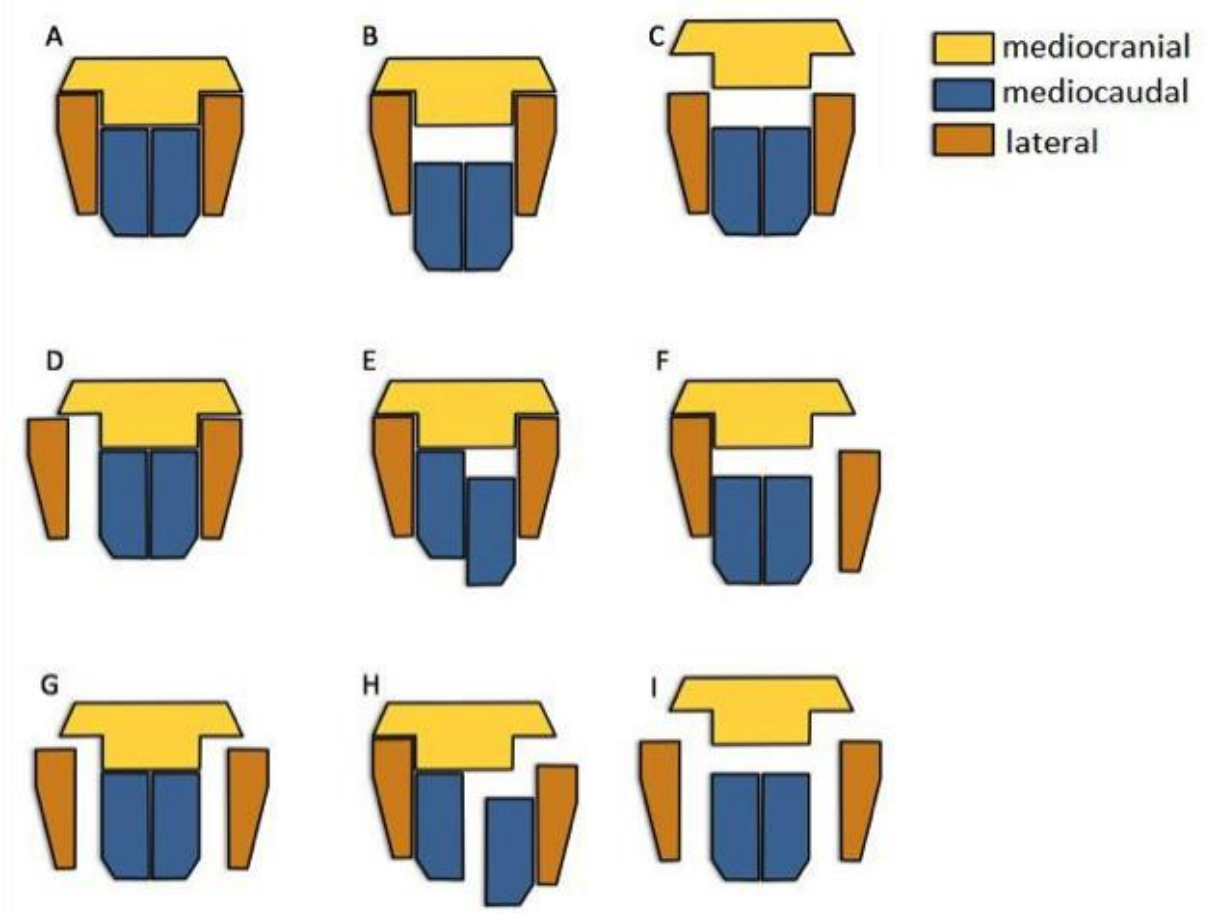

Figure 15. Presternal patterns showing different spatial relationships among the same five elements.

2.2. Comparative micro CT scans. Ten presterna of fossil and extant species from basal eutherian orders were obtained as loans from three lending institutions: Arizona Western College, Yuma, AZ (AWC), the University of Florida, Gainesville, FL (UF), and the Museum of Comparative Zoology, Cambridge, MA (MCZ) (Table1). The comparative taxa were selected based on three criteria: suggestion of external partitioning, as seen in *Paramylodon harlani*, basal phylogenetic position, and variation in use of the forelimb. The specimens were microCT scanned by Aaron Nakasone using ZEISS Xradia 520 Versa at the Photonics Lab at Boston University, MA (Table 1).

The thickness of scanned slices ranged between 13.9 um to 53.8 um, depending on the size of the specimen. Similar to medical CT scans, the micro-CT scans give the user the ability to study the interior of a structure by preserving the specimen without the need to cut the sample. The advantage of the micro-CT scan over the medical CT scan comes from its ability to image on a much smaller scale, giving a greatly increased resolution of nano-to-micrometers that is optimal for studying bone histology (http://microphotonics.com). The comparative microCT scans were visualized using the NIH software Fiji (Fiji Is Just ImageJ, Version Java 8).

The Dynamic Reslice plug-in of Fiji was used to draw an orthogonal slice through the visualized stacks (https://imagej.net/Dynamic_Reslice). This allowed the plane of the scan to be changed. Because the presternum is quite flat and thin, the coronal (frontal) plane was used to show the maximum area of element interface. Regions of interest (ROIs) were selected on either side of the element boundaries or in areas of distinctive trabecular structure for histological analysis. Care was taken to sample all three elements from a single slice by selecting multiple ROIs. If that was not possible, due to the curvature of the presternum, more slices were generated and an ROI corresponding to the element of interest was selected. Cortical bone on the outside of the element was avoided. Comparison of the tomographic images to photographs of the presterna were used to localize the position of ROIs.

The OrientationJ plug-in of Fiji was used to characterize orientation and isotropy of the trabeculae in each ROI. Distribution and Dominant Direction functionalities of the program were used. The Distribution function allowed for the automated evaluation of the orientation of each pixel storing it in a structure tensor, a matrix which represents partial derivatives and is commonly used in the field of image processing (Rezakhaniha et al., 2012). The total number of computer-generated frequencies per ROI ranged from 216 to 25220. The Distribution function generated a two-dimensional histogram: the x-axis of the histogram showed the orientation of pixels in degrees with a value between -90 and 90, and the y-value showed the frequency of each degree. Rose diagrams were then generated based on the data from Distribution. The frequencies for the 180 degrees were grouped and summed in bins of 10 consecutive degrees. The 18 bins were then plotted in R using ggplot2. The non-parametric Watson-Wheeler test was used to determine the statistical differences in the angular distributions of pairs of ROIs. This test was run on both 180 individual degree bins and on the 18 grouped degree bins. The Dominant Direction function generated two values - dominant direction and coherency. The dominant direction indicates the preferred orientation of the majority of the pixels in the ROI. In this case it is the dominant direction of the trabeculae. Coherency evaluated isotropy of the local structure on a scale between 0 and 1. A value closer to 1 indicates a dominant direction (anisotropy), whereas a value closer to 0 indicates isotropy and a uniform distribution of fibers in every direction.

The BoneJ plug-in of Fiji was used to measure the ratio of bone to the total area in an ROI and is represented as percent bone here (Doube et al. 2010).

Table 1. Comparative species micro scanned for histological analysis. F/E = fossil / extant. Institutional abbreviations: AWC = Arizona Western College; MCZ = Museum of Comparative Zoology; UF = University of Florida; WC = Wellesley College.

Order	Picture	Species	Common Name	Lifestyle	F/E	Museum Number
Pilosa		Tamandua tetradactyla	collared anteater	arboreal/ knuckle-walking	E	MCZ 1023
		Tamandua tetradactyla	collared anteater	arboreal/ knuckle-walking	E	MCZ 34961
		Nothrotheriops texanus	ground sloth	arboreal/ knuckle-walking	F	AWC 22949
Cingulata		Dasypus bellus	armadillo	burrower	F	UF 224700
		Cabassous tatouay	greater naked -tailed armadillo	burrower	E	MCZ 1021
Eulipotyphla		Erinaceous europaeus	hedgehog	burrower	E	MCZ 25884
		Solenodon paradoxus	---	burrower	E	MCZ 12381
Chiroptera		Eidolon dupreanum	madagascar fruit bat	active flight	E	MCZ 45068
Primates		Gorilla gorilla gorilla	---	knuckle-walking	E	MCZ 26850
	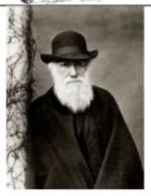	Homo sapiens	human	bipedal walking	E	WC, uncat.

3. Results

The 351 human thoracic CT scans obtained from Wake Forest University were used to generate 3D images, which were then evaluated for evidence of composite presternal structure. Each presternum was assigned to one of nine pattern categories based on element location and articulating structures (Figures 16-22). Only seven of the nine possible patterns were observed (Table 2). The great majority of the scans (312 of 351), including all specimens from individuals over 10 years of age, show a default structure, identified as pattern A, with no subdivision of the presternum. The remaining individuals displayed two or more internal elements that are variously fused and not yet fully integrated into the major structural unit. The average age in years of these remaining six pattern categories was less than 4 years-old, and none of the individuals was older than 10 years old (Table1).

Table 2. Pattern distribution by number of scans and average age in years. Patterns C and G were not observed in our dataset.

Pattern	Average Age (years)	Number of individuals
A	33.24	309
B	1.01	19
C	X	0
D	3.17	3
E	3.72	8
F	0.69	3
G	X	0
H	1.92	1
I	0.48	3

3.1. Presternal Patterns. Pattern A is represented by 309 individuals, or 88.8% of the dataset (Table 2). No composite elements are visible, and all three distal structures articulate directly with the main body of the presternum (Fig. 16). Two individuals of pattern A have more than one scan and are described below in more detail. All remaining patterns show composite structure: i.e., there are at least two elements visible in the presternum.

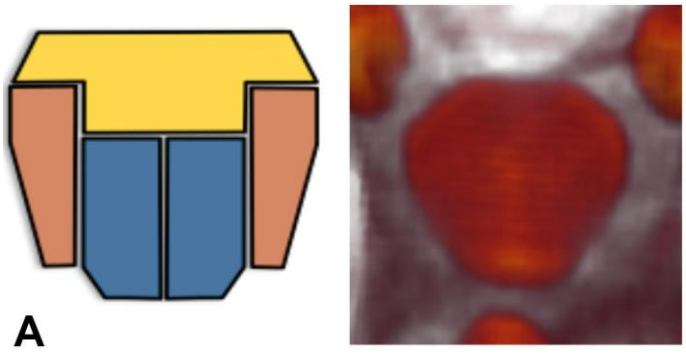

Figure 16. Pattern A, illustrated by individual W017, aged 2.84 years.

Pattern B is represented by 19 individuals, or 5.41% of the dataset (Table 2). This pattern represents a separation of both members of the mediocaudal element pair from both the mediocranial and lateral elements, which are united anteriorly. The default articulation relationships of the mediocaudal element with the the second thoracic rib (laterally) and the first sternebra (posteriorly) are retained. Importantly, the mediocaudal element can be either paired (individual W771) or unpaired (individual W650) (Fig. 17). See pattern E below for individuals with only one of the paired mediocaudal elements displaced. The average age in this group is 1.01 years.

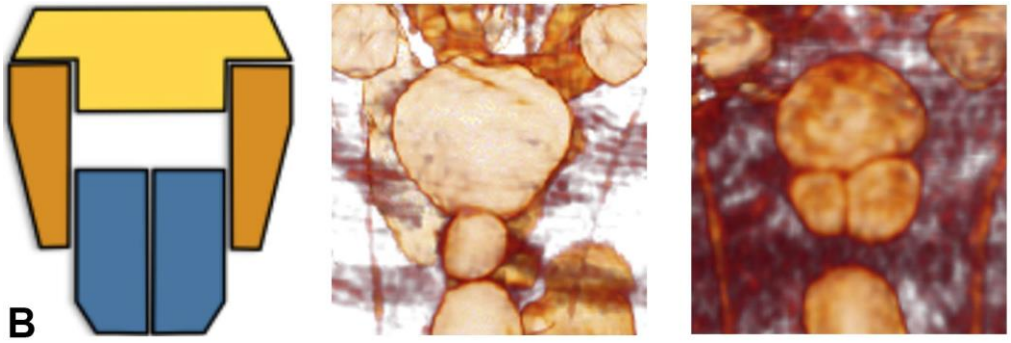

Figure 17. Pattern B, illustrated by individual W650 (aged 2.60 years, middle) and individual W771 (aged 0.72 years, right). Average age in this group is 1.01 years.

Pattern D is represented by 3 individuals, or 0.85% of the dataset (Table 2). This pattern represents a separation of one of the lateral elements. The default articulation relationship with the first thoracic rib is preserved. Individual W016 shows a clear articulating pattern (Fig. 18). The average age in this group is 3.17 years.

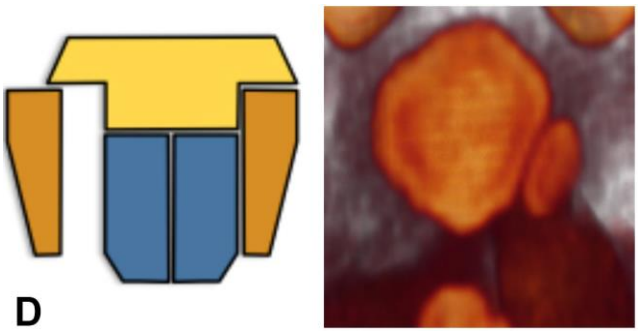

Figure 18. Pattern D illustrated by individual W016, aged 2.13 years. Average age of the group is 3.17 years.

Pattern E is represented by 8 individuals, or 2.29% of the dataset (Table 2). This pattern represents a separation of only one of the members of the mediocaudal elements. The default articulation relationships mentioned above are observed here as well. Individual W830 shows a clear articulating pattern (Fig. 19). The average age in this group is 3.72 years.

Figure 19. Pattern E illustrated by individual W830, aged 3.82 years. Average age of the group is 3.72 years.

Pattern F is represented by 3 individuals, or 0.85% of the dataset (Table 2). This pattern represents a separation of the mediocaudal element(s) and also one of the lateral elements. The default articulation relationships are observed here as well. Individual W681 shows a clear articulating pattern (Fig. 20). The average age in this group is 0.69 years.

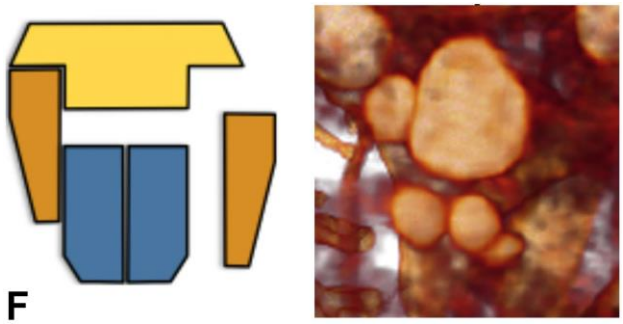

Figure 20. Pattern F, illustrated by W681, aged 0.33 years. Average age of the group is 0.69 years.

Pattern H is represented by only 1 individual, or 0.57% of the dataset (Table 2). This pattern represents a segmentation of one of the paired mediocaudal and lateral elements on the same side. The default articulation relationship mentioned above is observed here as well. Individual W622 shows a clear articulating pattern (Fig. 21). The age of the individual is 1.49 years old. A longitudinal observation of this individual is described in the subsequent section.

Figure 21. Pattern H is illustrated by a single individual, W622D, age 1.49 years.

Pattern I is represented by 3 individuals, or 0.85% of the dataset (Table 2). This pattern represents a separation of the medicranial, the paired mediocaudal, and the lateral elements from each other. The default articulation relationship to each of the elements mentioned above is preserved. Individual W762 shows a clear articulating pattern (Fig. 22). The average age in this group is 0.48 years.

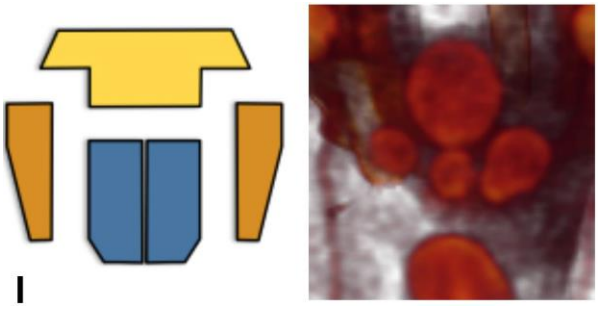

Figure 22. Pattern I is observed in three individuals and is illustrated by W849, age 0.72 years. Average age in the group is 0.48 years.

The trends above are graphed in Fig. 23 demonstrating the age range for each pattern with the maximum and minimum age. Additionally, patterns were ordered based on either average age or maximum age within the pattern (Table 3). The number of elements segmented and the identity of those elements were evaluated (Table 3). The range of ages within each pattern and the identity of the separated elements is summarized in the figure (Fig. 23) and the table (Table 3) below.

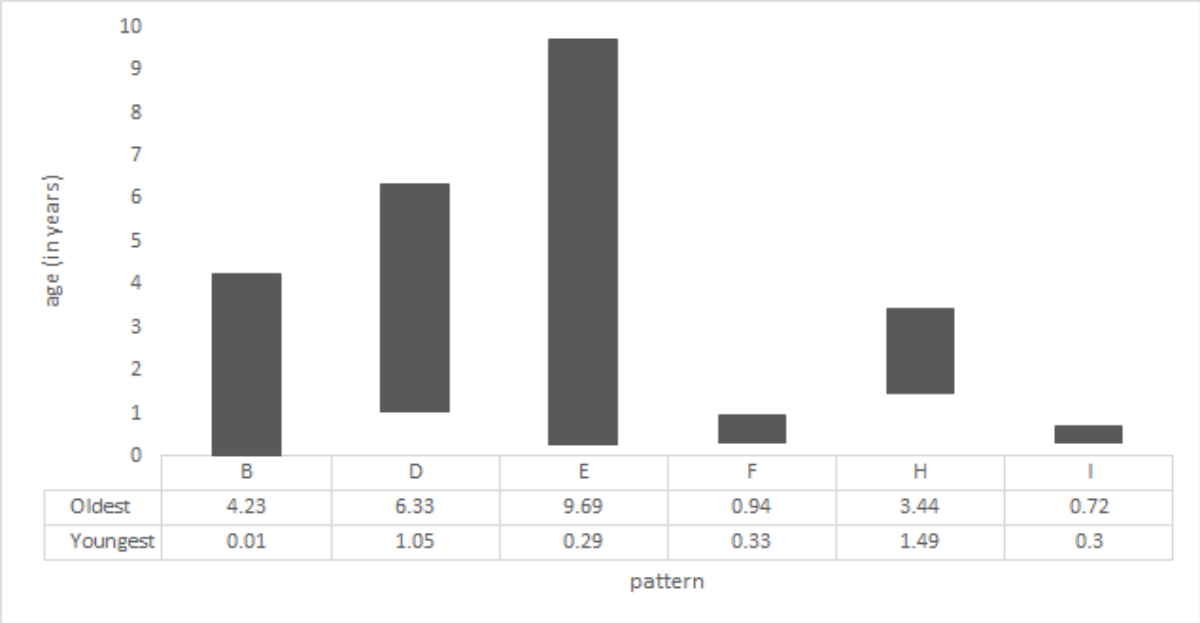

Figure 23. Age range patterns B through I in the Weaver database. Pattern A is not included in this figure as it is represented in all age groups (0-99 years). The oldest and youngest individual of each of the other patterns was selected and the age range within each pattern is shown.

Table 3. Rank order of patterns based on average age (in years) in each group (left) and according to the oldest individual (in years) in the group (right).

Pattern	Average Age	# and identity of units separated	Pattern	Maximum Age	# and identity of units separated
I	0.48	2 lateral 2 caudal	I	0.72	2 lateral 2 caudal
F	0.69	1 lateral 2 caudal	F	0.94	1 lateral 2 caudal
B	1.01	2 caudal	H	3.44	1 lateral 1 caudal
H	1.92	1 lateral 1 caudal	B	4.23	2 caudal
D	3.17	1 lateral	D	6.33	1 lateral
E	3.72	1 caudal	E	9.69	1 caudal
A	33.24	0	A	97.32	0

3.2. Ontogenetic changes within presternal patterns. The lack of individuals with multiple presternal elements over the age of 10 indicates that presternal fusion, whatever its sequence and patterns, is completed by the age of 10 (Fig. 24). Additionally, the Weaver database contains three ontogenetic series that show changes in sternal anatomy in a single individual with age (Figs. 25-27). Finally, the many individuals with pattern A also demonstrate the typical ossification changes after fusion is complete (Fig. 28).

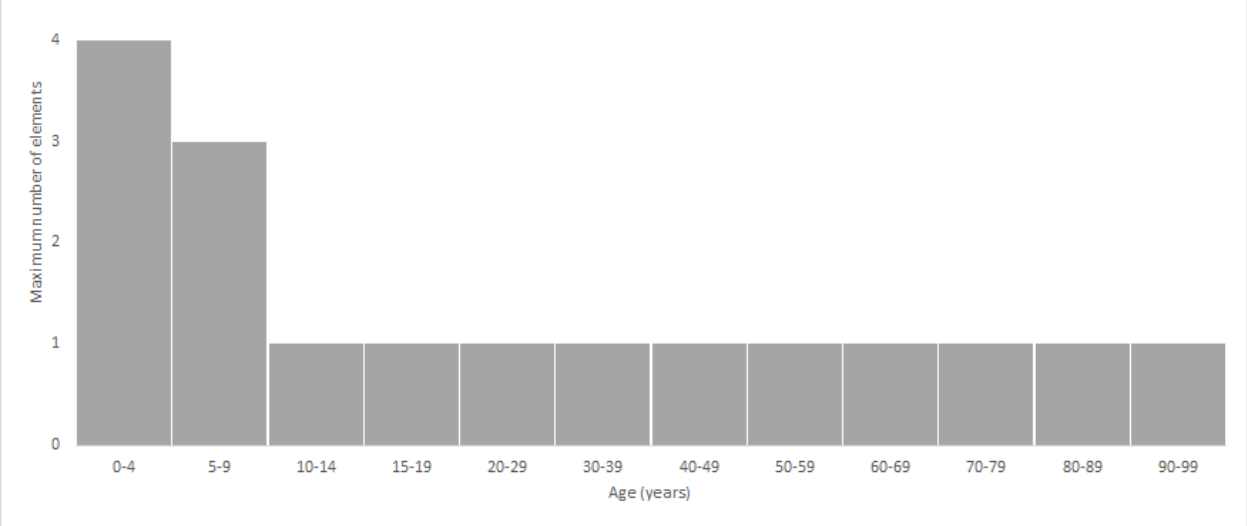

Figure 24. Maximum number of elements observed in individuals within 10-year age bins. For ages 0 - 20, each bin represents a range of 5 years; for years 20 - 99, each bin represents a range of 10 years.

Three individuals had multiple scans taken at different periods of time. These scans provided an additional observation on the development of the presternum over time. The presterna of the three individuals were assigned to the patterning mentioned above.

Individual W004 belongs to pattern A and has CT scans taken at 0.74 and 0.89 years old. The mediocranial, mediocaudal, and lateral elements are not separated and are assembled within the main structure. There is a minor lateral expansion of the presternum in the scan taken at the older age (Fig. 25). The presternal elements show the default articulation with the marginal structures.

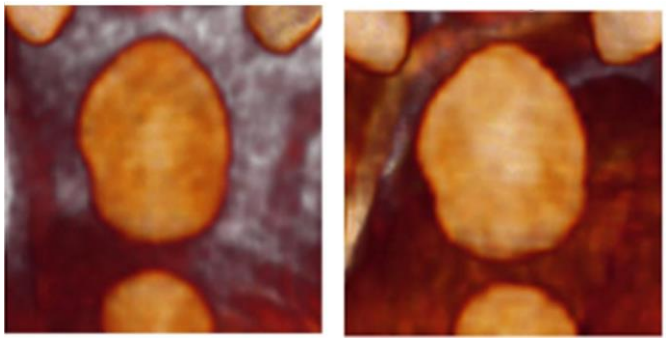

Figure 25. Two scans of individual W004, assigned to pattern A. The scans were taken at 0.74 (left) and 0.89 (right) years of age.

Individual W642 also belongs to pattern A and has CT scans taken at 0.3, 0.47, 1.28, 1.87 years of age. The mediocranial, mediocaudal, and lateral are not separated and are assembled within the main structure. With an increase in age, a lateral expansion of the presternum is visible. (Fig. 26). The presternal elements show the default articulation with the marginal structures.

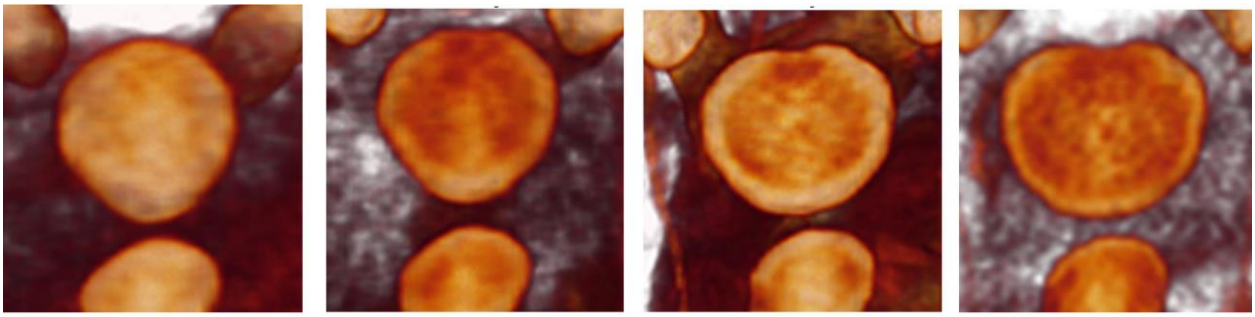

Figure 26. Four scans of individual W642, assigned to pattern A. The scans were taken at ages of 0.30, 0.47, 1.28, and 1.87 years, from left to right.

Individual W622 belongs to pattern H and has CT scans taken at 1.49 and 3.44 years old. One of the mediocaudal, and one of the lateral elements are separated from the main structure. With an increase in age, an expansion of the presternum is visible. In addition, there is an increase in the length of the contact zone between the main structure and the separated element (Fig. 27). The presternal elements all show default articulations with the marginal structures.

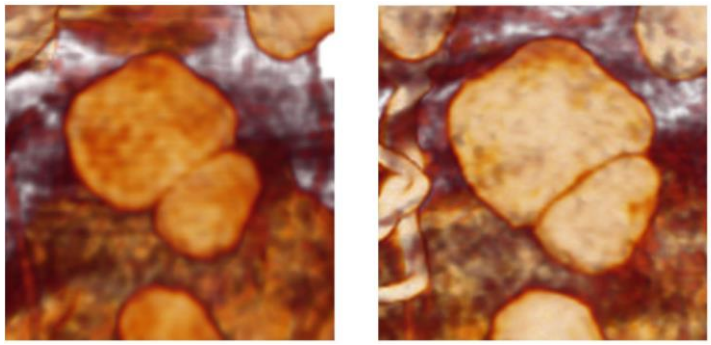

Figure 27. Two scans of individual W622, assigned to pattern H. The scans were taken at 1.49 (left) and 3.44 (right) years of age.

Pattern A individuals of different age allowed documentation of ossification during ontogeny (Fig. 28). With progression of age, there is an expansion of the presternum, as well as progressive ossification of the lateral ribs and elimination of space between the articulating structures and their respective elements. In some cases, the presternum extends to and fuses with the mesosternum and the xhiphisternum as in individual W564, aged 74.56 years (Fig. 29 (who is also individual 8 from Fig. 28)).

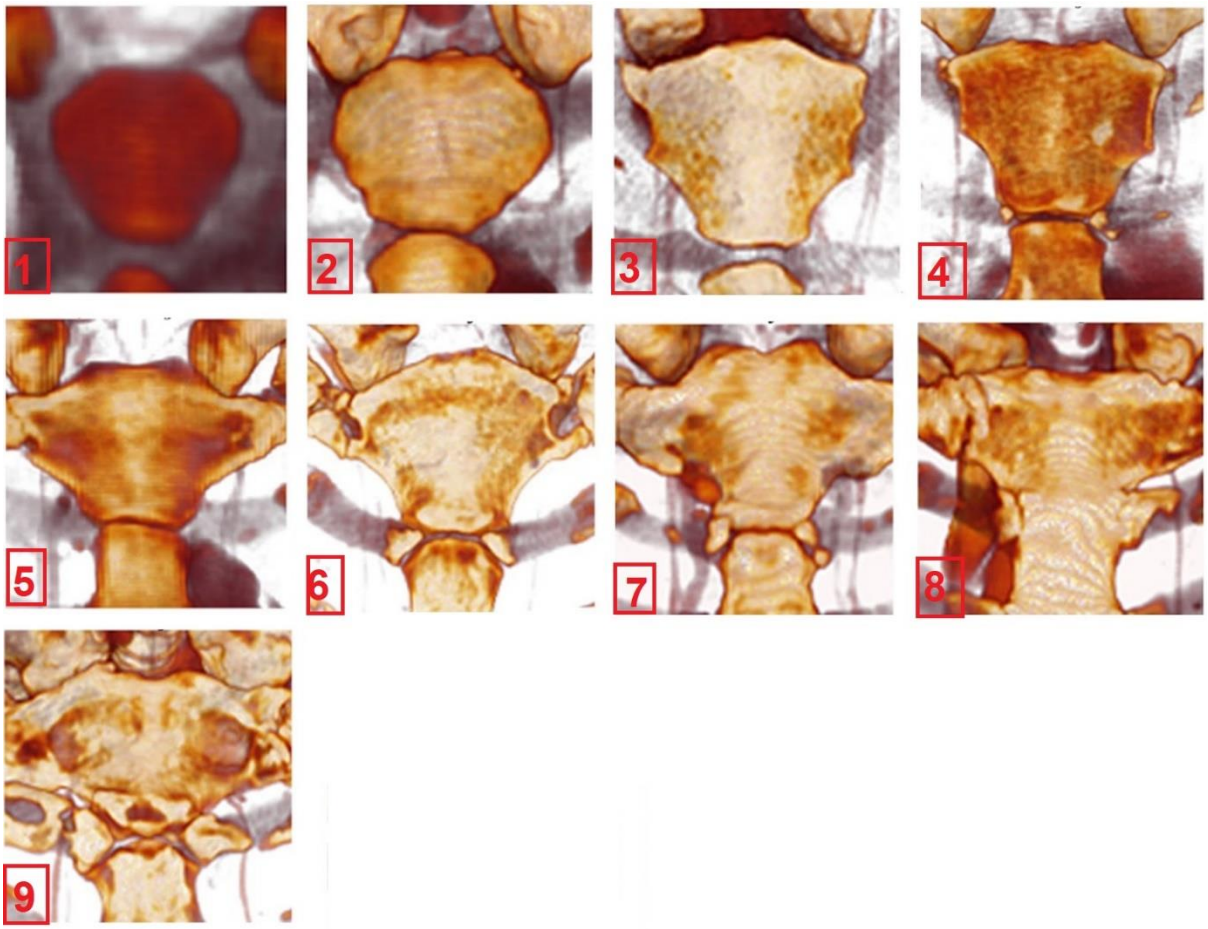

Figure 28. Variation in presternal structure by decade of age ofindividuals assigned to Pattern A. The average age of each 10-year age bin was taken and the individual whose age most closely matched the mean age was illustrated. Top row ages are 2.84, 15.14, 24.29, and 35.21 years, left to right. Middle row ages are 45.44, and 54.74, 65.19, and 74.56 years, left to right. The age of the individual in the bottom row is 84.18 years.

Figure. 29. Individual W564, aged 74.56 years showing an ossification of all sternal component parts and partial ossifications of the ribs to the sternum.

3.3. Comparative Sternal Series. The work of Feldman (2017) indicated that presterna of adults of the fossil ground sloth *Paramylodon harlani* are sometimes composite. The presence of multiple elements in adults could be unique to the Order Xenarthra, which is considered among the most basal eutherian placentals, or could be more widely distributed. Comparative taxa were therefore examined using microCT scans to ask if composite structure might exist within other eutherians, even if cryptic or unrecognizable from the external anatomy of adults. Possible indicators might consist of a physical separation such as an internal seam, or a difference in trabecular orientation, percent bone, and/or degree of anisotropy, all characteristic measures of cancellous bone (Kivell, 2016).

Of the specimens surveyed, some show an overt separation, others a cryptic separation, and still others show no physical barrier between presternal elements of any kind. All presterna show bilateral symmetry, therefore any interpretation done on one side applies to its mirror image on the other side. Species were analyzed in the order they appear in Table 1 and documented in Fig. 30. The additional descriptors of the histology – dominant direction, coherency, and bone density - are reported in Table 4.

Figure 30 (below). Comparative sternal series. For each species the top panel shows a photo of the presternum and pictures of the micro CT scan slice/s chosen for analysis in Fiji with red squares put around each ROI. The bottom panel shows trabecular orientation data of each ROI. The first column shows ROI number and the corresponding element. The second column gives the results of a statistical comparison between slices using the Watson Wheeler non-parametric test. The third column shows rose diagrams created using R. For this circular representation of the data, the values between 0 and 179 degrees were were replicated between 180 and 359 degrees. The fourth column shows the histograms generated by the OrientationJ menu of ImageJ. The distribution of degrees of orientation of trabeculae in selected ROIs is presented. Scale size in all images equals 5 mm except for *Gorilla and Homo*, in which it equals 10 mm. *Nothrotheriops texanus* is not included in this figure.

Tamandua tetradacyla (MCZ 1023) Collared anteater

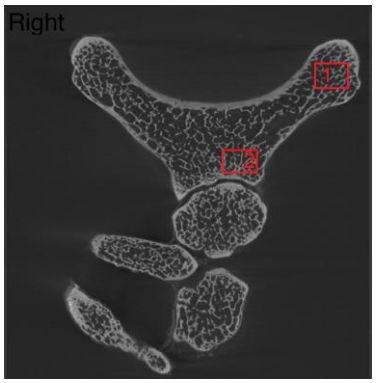

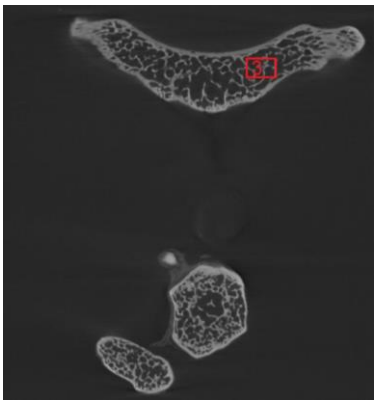

ROI/element	Statistical Significance	Rose Diagrams	Histograms
ROI 1 / lateral	ROI 1 vs ROI 2 $p < 0.001$ ROI 1 vs ROI 3 $p < 0.001$ ROI 2 vs ROI 3 $p < 0.001$	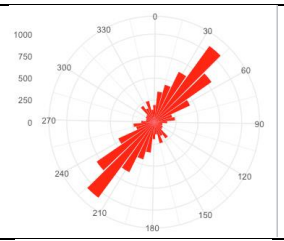	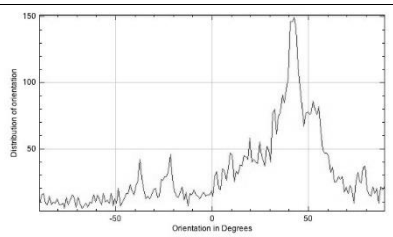
ROI 2/ mediocaudal		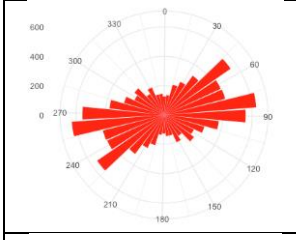	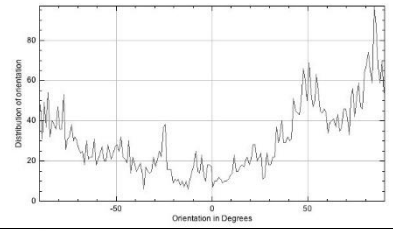
ROI 3 / mediocranial		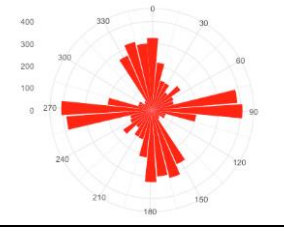	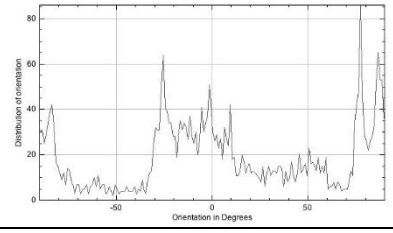

***Tamandua tetradactyla* (MCZ 34961) Collared anteater**

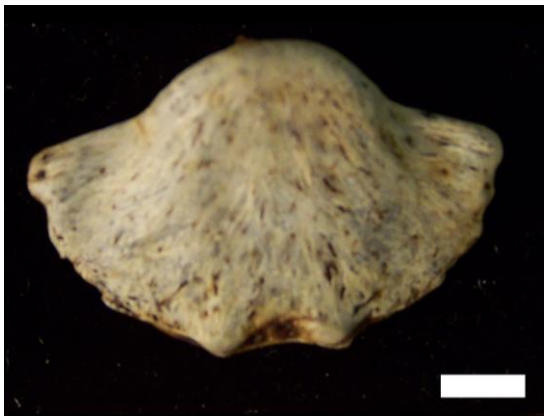

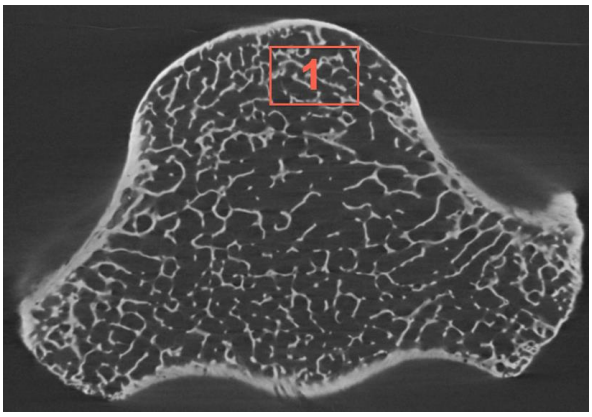

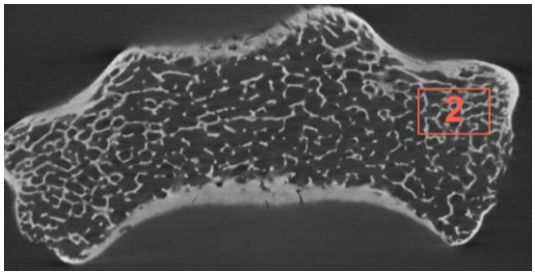

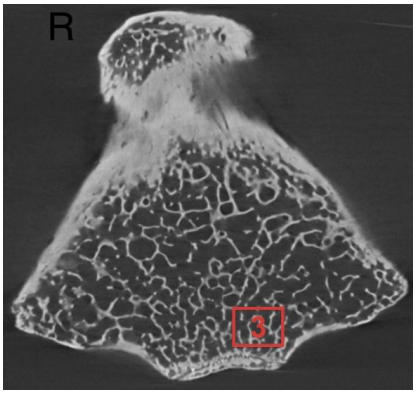

ROI	Statistical Significance	Rose Diagrams	Histograms
ROI 1 / mediocranial	ROI 1 vs ROI 2 p < 0.001 ROI 1 vs ROI 3 p < 0.001 ROI 2 vs ROI 3 p < 0.001	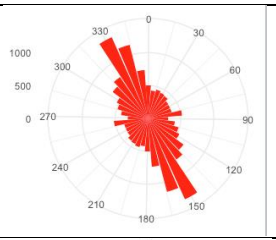	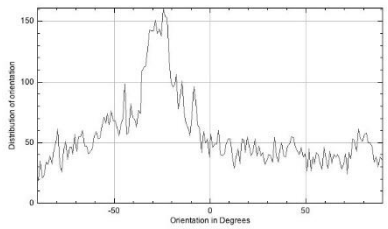
ROI 2 / lateral		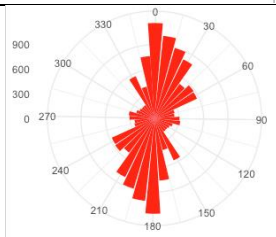	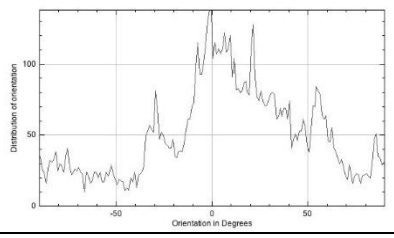
ROI 3 / mediocaudal		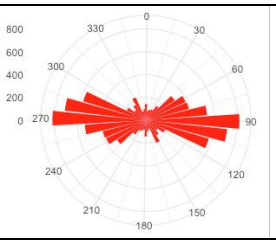	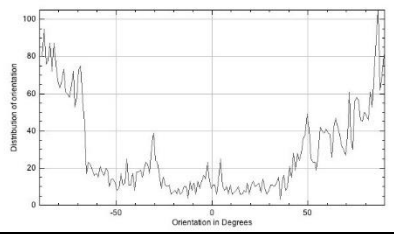

***Dasypus bellus* (UF 224700) –**

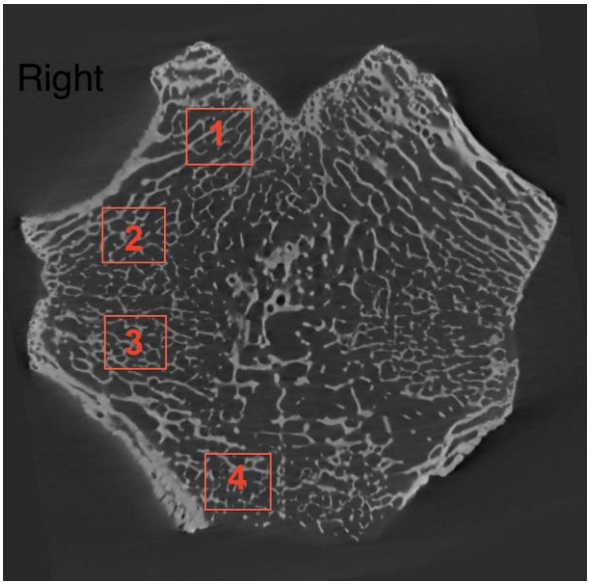

ROI	Statistical Significance	Rose Diagrams	Histograms
ROI 1 / mediocranial	ROI 1 vs ROI 2 p < 0.001	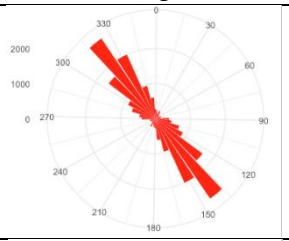	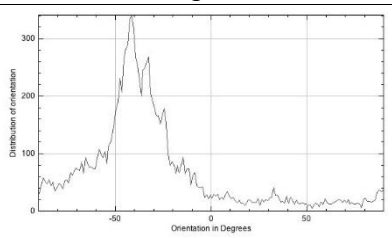
ROI 2 / lateral	ROI 1 vs ROI 3 p < 0.001 ROI 1 vs ROI 4 p < 0.001	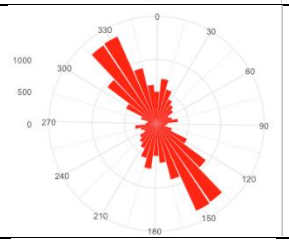	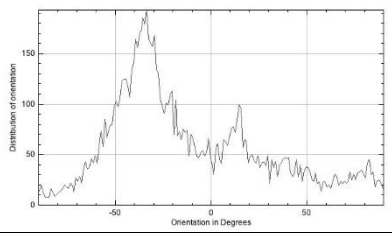
ROI 3 / lateral	ROI 2 vs ROI 3 p < 0.001 ROI 2 vs ROI 4 p < 0.001	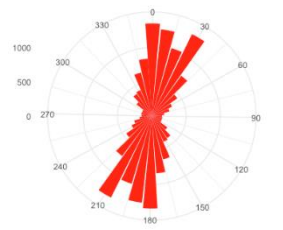	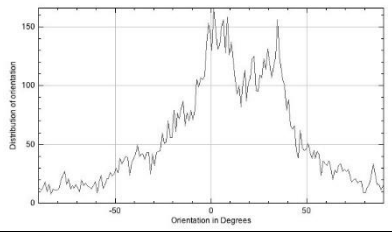
ROI 4 / mediocaudal	ROI 3 vs ROI 4 p < 0.001	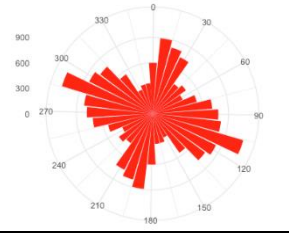	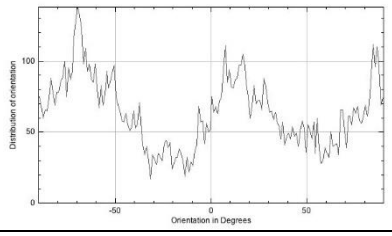

Cabassous tatouay (MCZ 1021) Greater naked-tailed armadillo

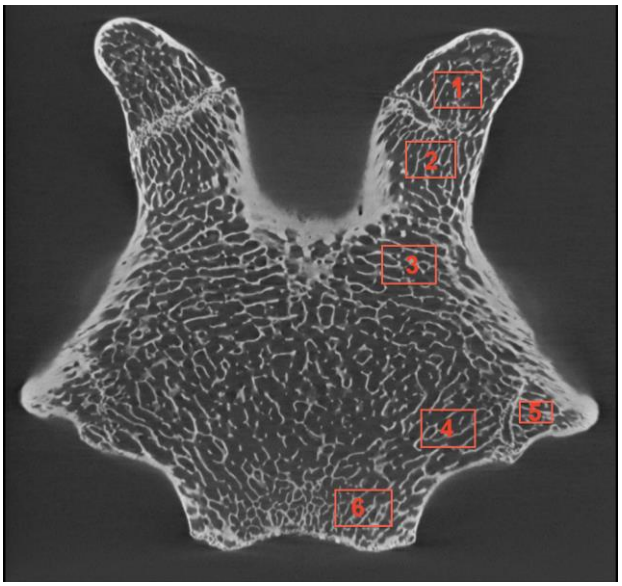

ROI	Statistical Significance	Rose Diagrams	Histograms
ROI 1 / mediocranial	ROI 1 vs ROI 2 p < 0.001 ROI 1 vs ROI 3 p < 0.001	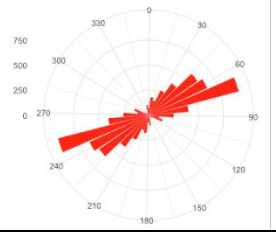	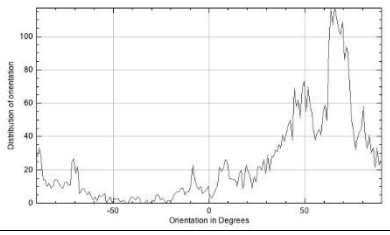
ROI 2 / mediocranial	ROI 1 vs ROI 4 p < 0.001 ROI 1 vs ROI 5 p < 0.001	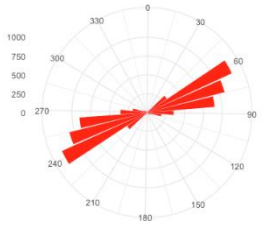	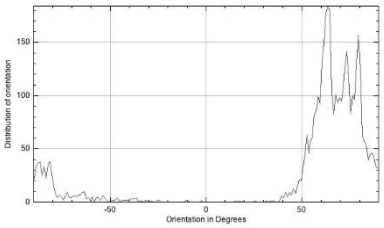
ROI 3 / lateral	ROI 1 vs ROI 6 p < 0.001 ROI 2 vs ROI 3 p < 0.001	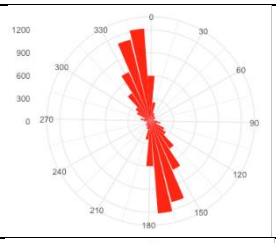	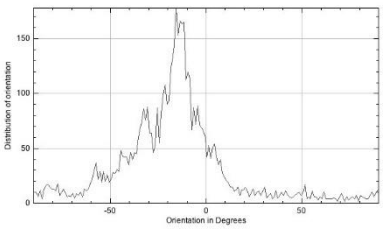
ROI 4 / lateral	ROI 2 vs ROI 4 p < 0.001 ROI 2 vs ROI 5 p < 0.001	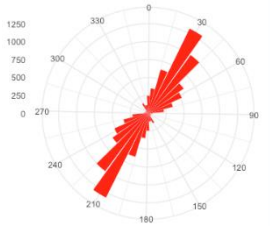	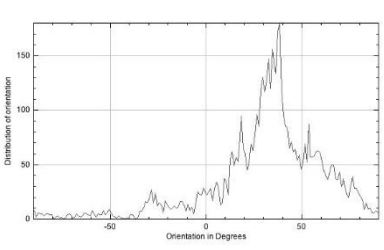

ROI 5 / lateral	ROI 2 vs ROI 6 p < 0.001 ROI 3 vs ROI 4 p < 0.001 ROI 3 vs ROI 5 p < 0.001 ROI 3 vs ROI 6 p < 0.001 ROI 4 vs ROI 5 p < 0.001 ROI 4 vs ROI 6 p < 0.001 ROI 5 vs ROI 6 p < 0.001	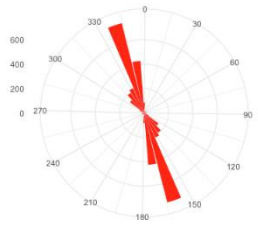	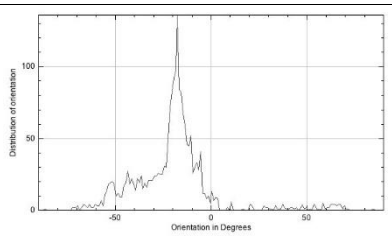
ROI 6 / mediocaudal		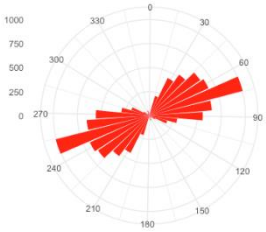	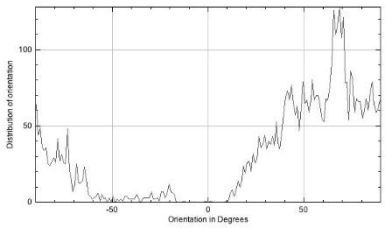

Erinaceous europaeus (MCZ 25884) hedgehog

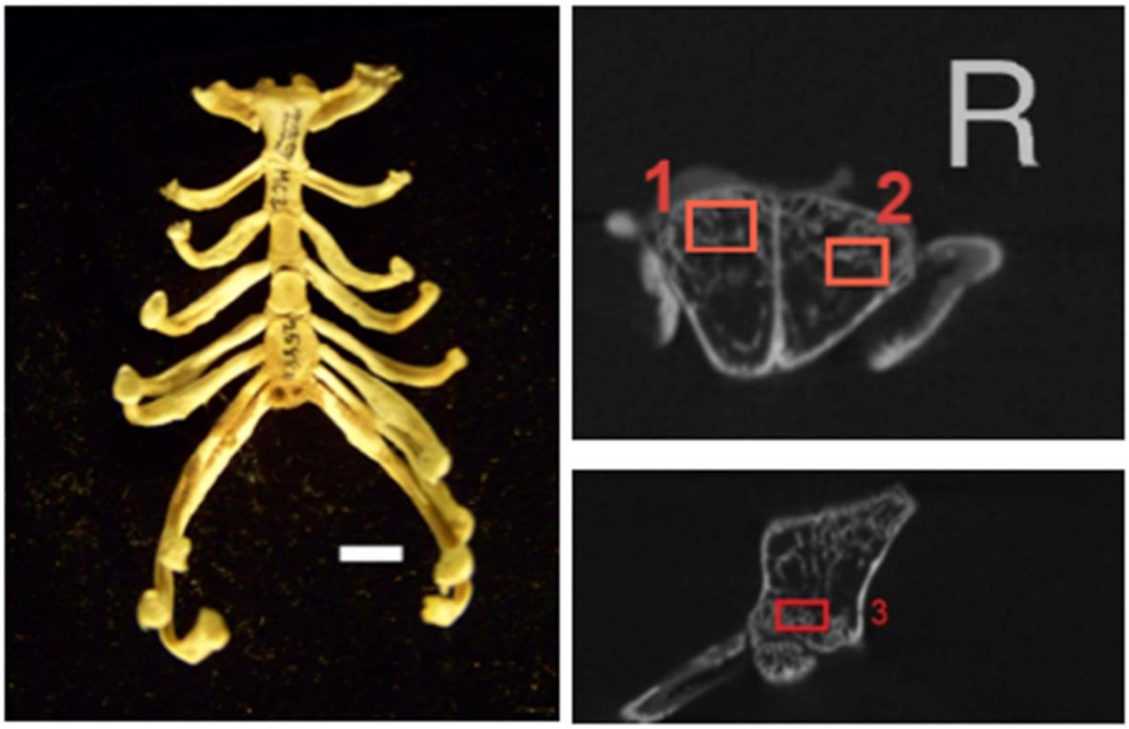

ROI	Statistical Significance	Rose Diagrams	Histograms
ROI 1/ mediocranial	ROI 1 vs ROI 2 p < 0.001 ROI 1 vs ROI 3 p < 0.001 ROI 2 vs ROI 3 p < 0.001	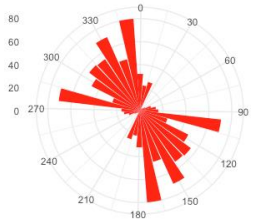	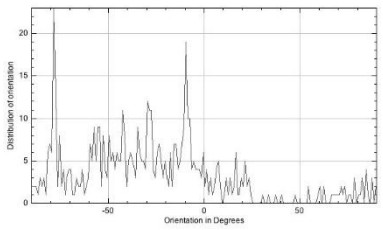
ROI 2 / lateral		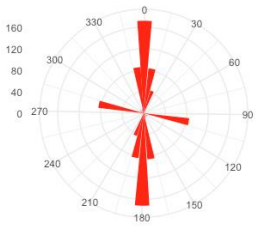	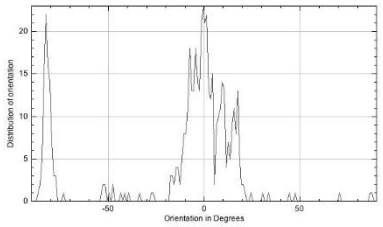
ROI 3 / mediocaudal		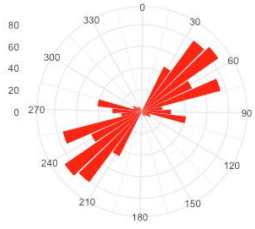	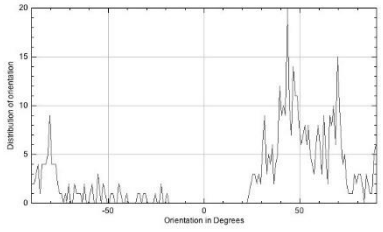

***Solenodon paradoxus* (MCZ 12381) --**

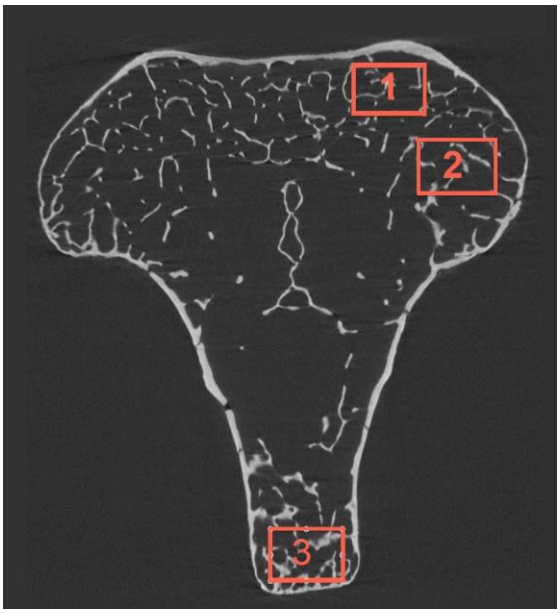

ROI	Statistical Significance	Rose Diagrams	Histograms
ROI 1/ mediocranial	ROI 1 vs ROI 2 p < 0.001 ROI 1 vs ROI 3 p < 0.001 ROI 2 vs ROI 3 p < 0.001	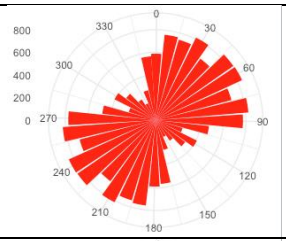	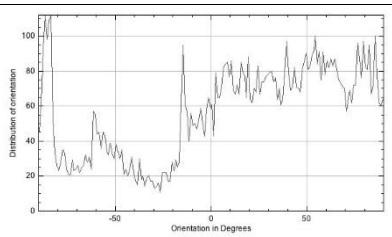
ROI 2 / lateral		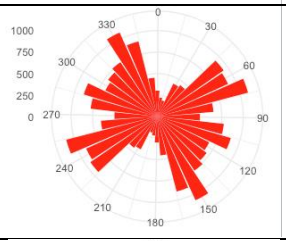	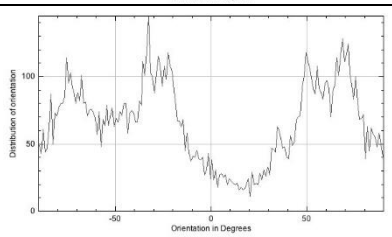
ROI 3 / mediocaudal		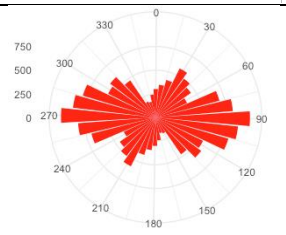	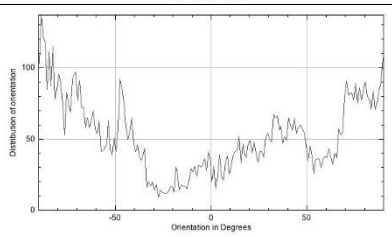

Eidolon dupreanum (MCZ 45068) Madagascar fruit bat

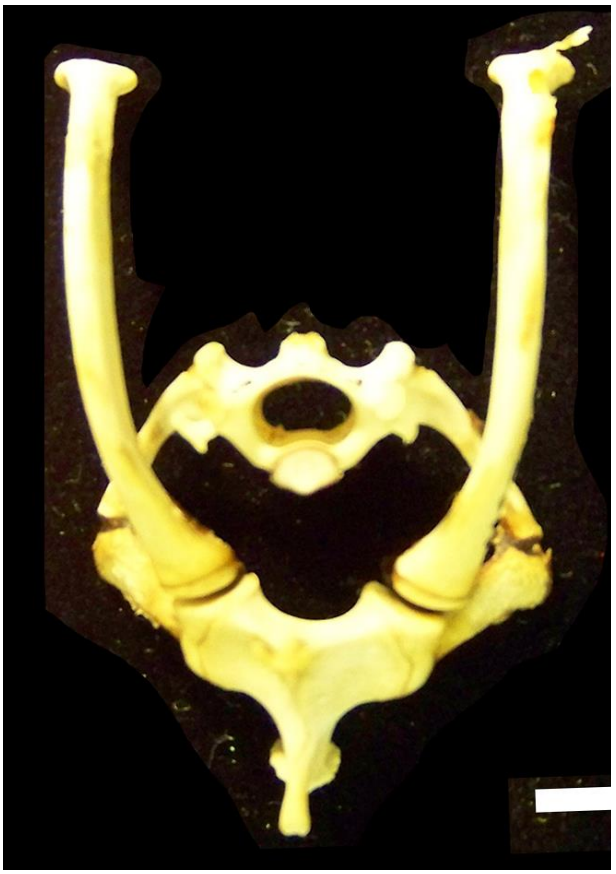

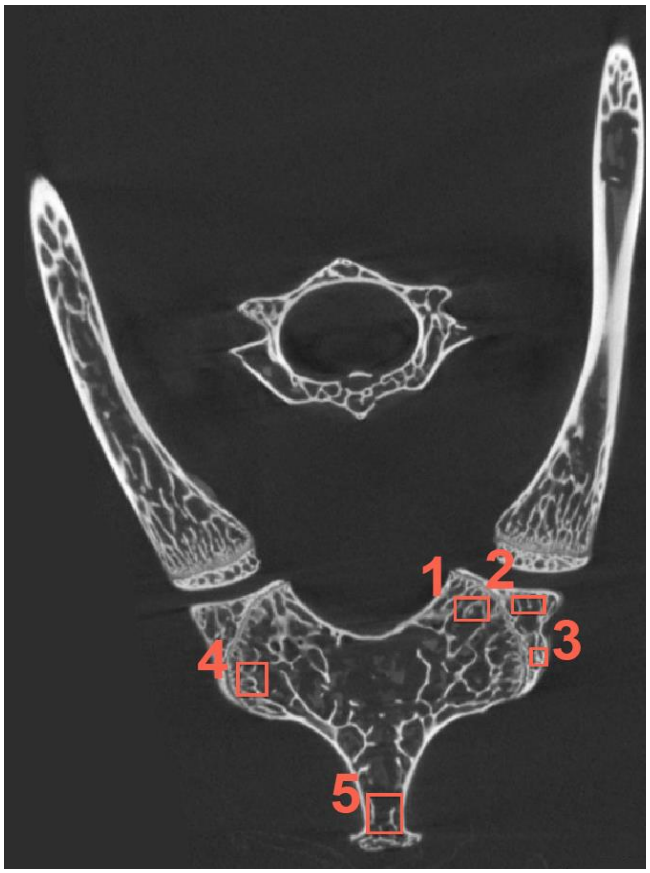

ROI	Statistical Significance	Rose Diagrams	Histograms
ROI 1 / medioranial	ROI 1 vs ROI 2 p < 0.001 ROI 1 vs ROI 3 p < 0.001	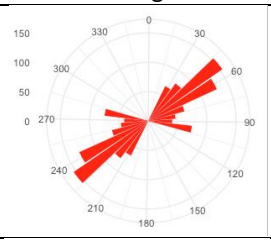	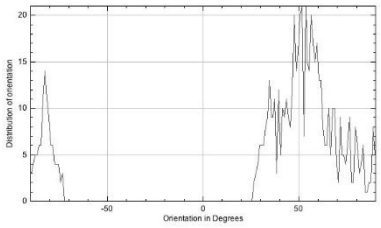
ROI 2 / medioranial	ROI 1 vs ROI 4 p < 0.001 ROI 1 vs ROI 5 p < 0.001	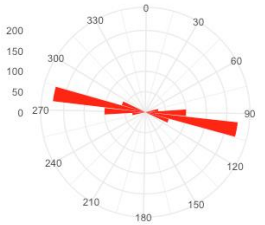	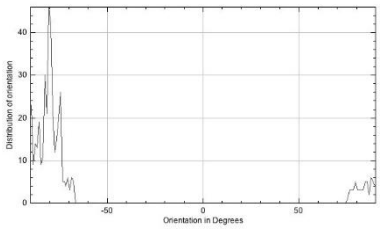

ROI 3 / lateral	ROI 2 vs ROI 3 p < 0.001 ROI 2 vs ROI 4 p < 0.001	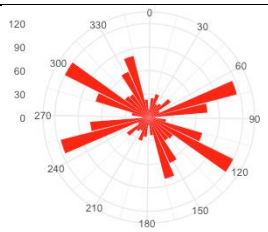	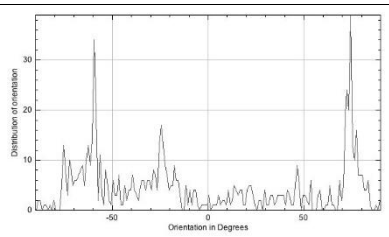
ROI 4/ lateral	ROI 2 vs ROI 5 p < 0.001 ROI 3 vs ROI 4 p < 0.001	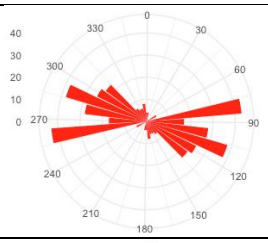	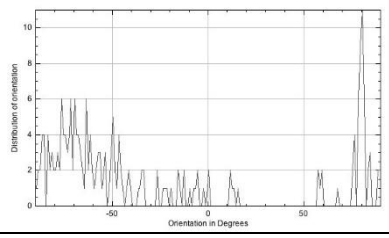
ROI 5/ mediocaudal	ROI 3 vs ROI 5 p < 0.001 ROI 4 vs ROI 5 p < 0.001	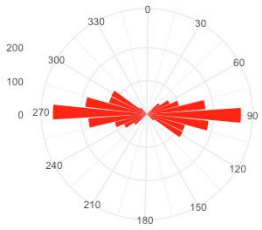	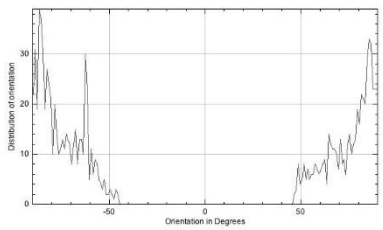

Gorilla gorilla gorilla (MCZ 26850) gorilla

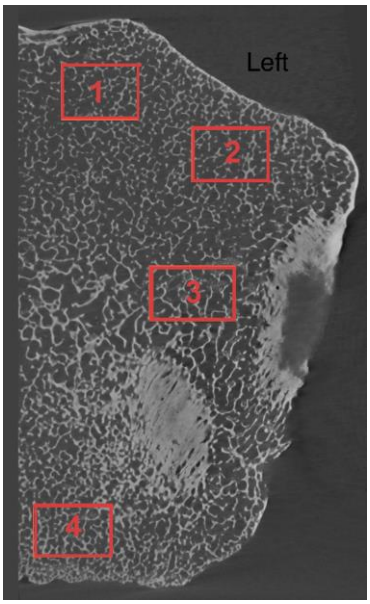

ROI	Statistical Significance	Rose Diagrams	Histograms
ROI 1 / mediocranial	ROI 1 vs ROI 2 p < 0.001 ROI 1 vs ROI 3 p < 0.001 ROI 1 vs ROI 4 p < 0.001 ROI 2 vs ROI 3 p < 0.001 ROI 2 vs ROI 4 p < 0.001 ROI 3 vs ROI 4 p < 0.001	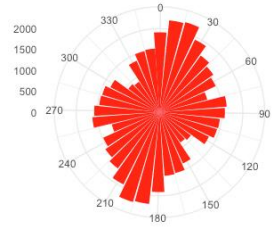	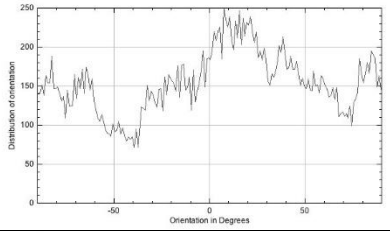
ROI 2 / lateral		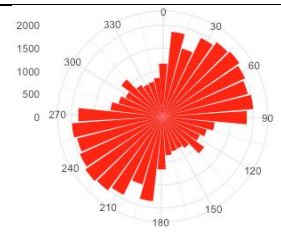	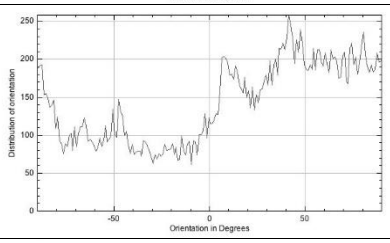
ROI 3 / lateral		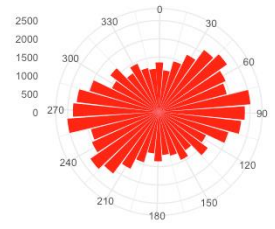	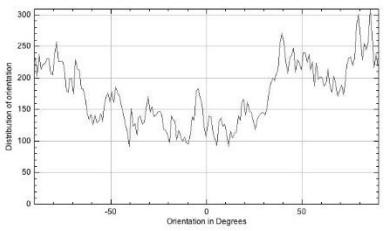
ROI 4 / mediocaudal		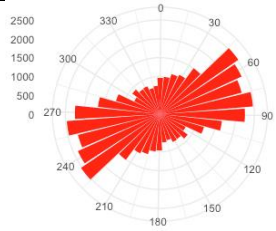	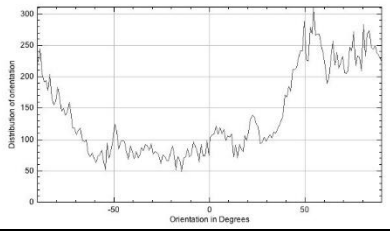

Homo sapiens (WC uncat.) human

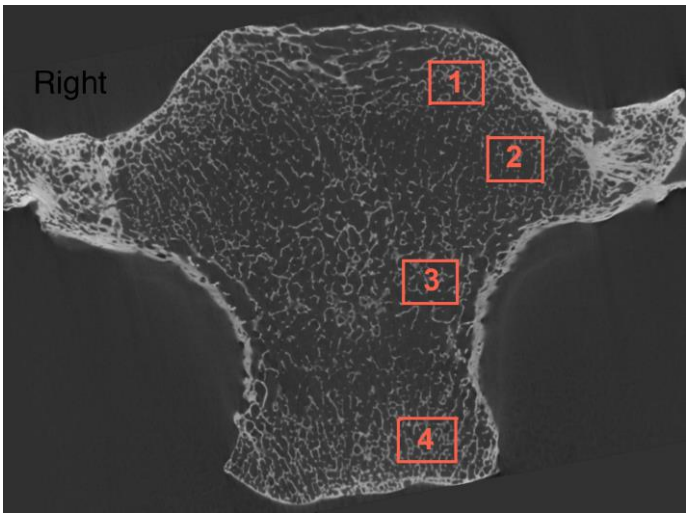

ROI	Statistical Significance	Rose Diagrams	Histograms
ROI 1 / mediocranial	ROI 1 vs ROI 2 p < 0.001	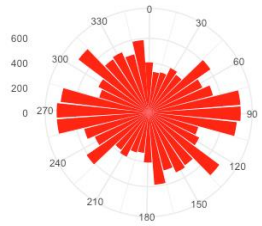	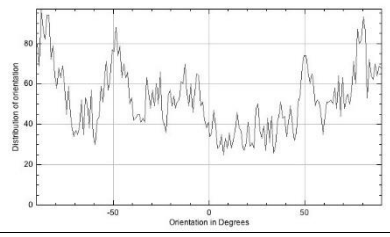
ROI 2 / lateral	ROI 1 vs ROI 3 p < 0.001 ROI 1 vs ROI 4 p < 0.001	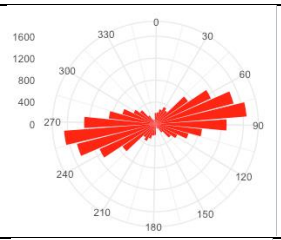	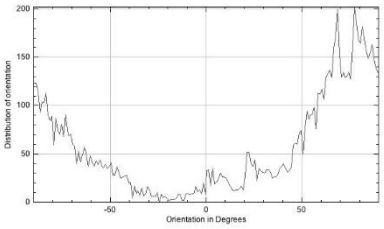
ROI 3 / lateral	ROI 2 vs ROI 3 p < 0.001 ROI 2 vs ROI 4 p < 0.001	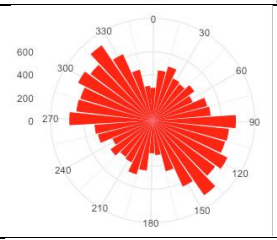	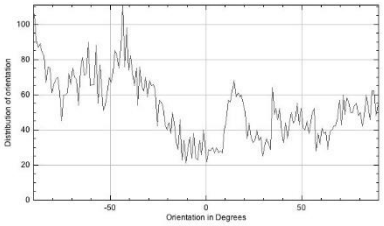
ROI 4 / mediocaudal	ROI 3 vs ROI 4 p < 0.001	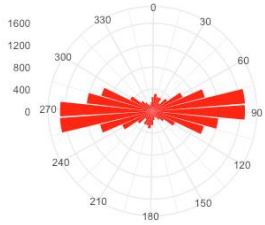	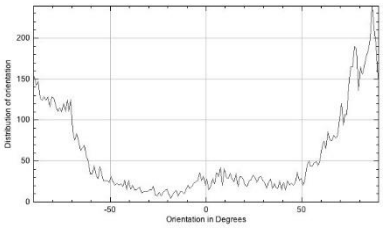

Table 4. Parameters for Dominant Direction (Dom Dir) in degrees, Coherency and % ratio of bone to total area (% ratio) for each ROI. Species name and museum number are provided. *Nothrotheriops texanus* is not included in this table.

Species Name/Museum #	ROI	Dom Dir	Coherency	% ratio
Tamandua tetradactyla MCZ 34961	1	-30.95	0.17	25.5
	2	16.82	0.27	28.8
	3	-89.82	0.35	21.7
Tamandua tetradactyla MCZ 1023	1	42.03	0.39	26.9
	2	73.89	0.21	32.5
	3	81.04	0.15	21.2
Dasypus bellus UF 224700	1	-41.81	0.49	25.7
	2	-27.03	0.29	21.5
	3	11.45	0.32	25.6
	4	-78.05	0.05	22.1
Cabassous tatouay MCZ 1021	1	64.59	0.49	17.6
	2	70.10	0.63	22.8
	3	-19.11	0.49	24.1
	4	36.96	0.50	20.3
	5	-21.97	0.66	31.3
	6	66.35	0.41	28.9
Erinaceous europaeus MCZ 25884	1	-36.59	0.20	39.4
	2	-2.45	0.34	34.7
	3	54.05	0.14	46.1
Solenodon paradoxus MCZ 12381	1	58.94	0.21	8.84
	2	-55.87	0.12	11.1
	3	-84.97	0.24	21.4
Eidolon dupreanum MCZ 45068	1	57.84	0.48	41.2
	2	-80.98	0.67	34.0
	3	-67.95	0.20	32.9
	4	-70.96	0.23	50.5
	5	-85.51	0.59	23.3
Gorilla gorilla gorilla MCZ 26850	1	60.92	0.075	18.1
	2	57.31	0.15	18.3
	3	85.04	0.21	19.8
	4	68.71	0.19	29.3
Homo sapiens WC uncat	1	-83.77	0.09	22.4
	2	74.93	0.35	15.3
	3	-59.69	0.026	15.8
	4	84.80	0.33	28.9

The data file containing the *Nothrotheriops texanus* CT scans was larger than the rest of the files and despite multiple attempts, the datafile caused repeated program crashes. The file contained 2172 slices or 16GB of information (as compared to a maximum of 1700 slices and 3.5GB of information for the other animals in Table 1). Dynamic reslice was beyond the

computing capabilities of Image J on the lab computer. Therefore, the cross-sections generated are as originally scanned and not in the frontal plane as for the remaining specimens. As a result, the *Nothrotheriops* scans were not included in the analysis of the comparative data. A cross-sectional image of *Nothrotheriops texanus* is provided showing overt boundaries. And still, even in the axial plane, three component parts can be recognized both externally and in cross-section (Fig.31).

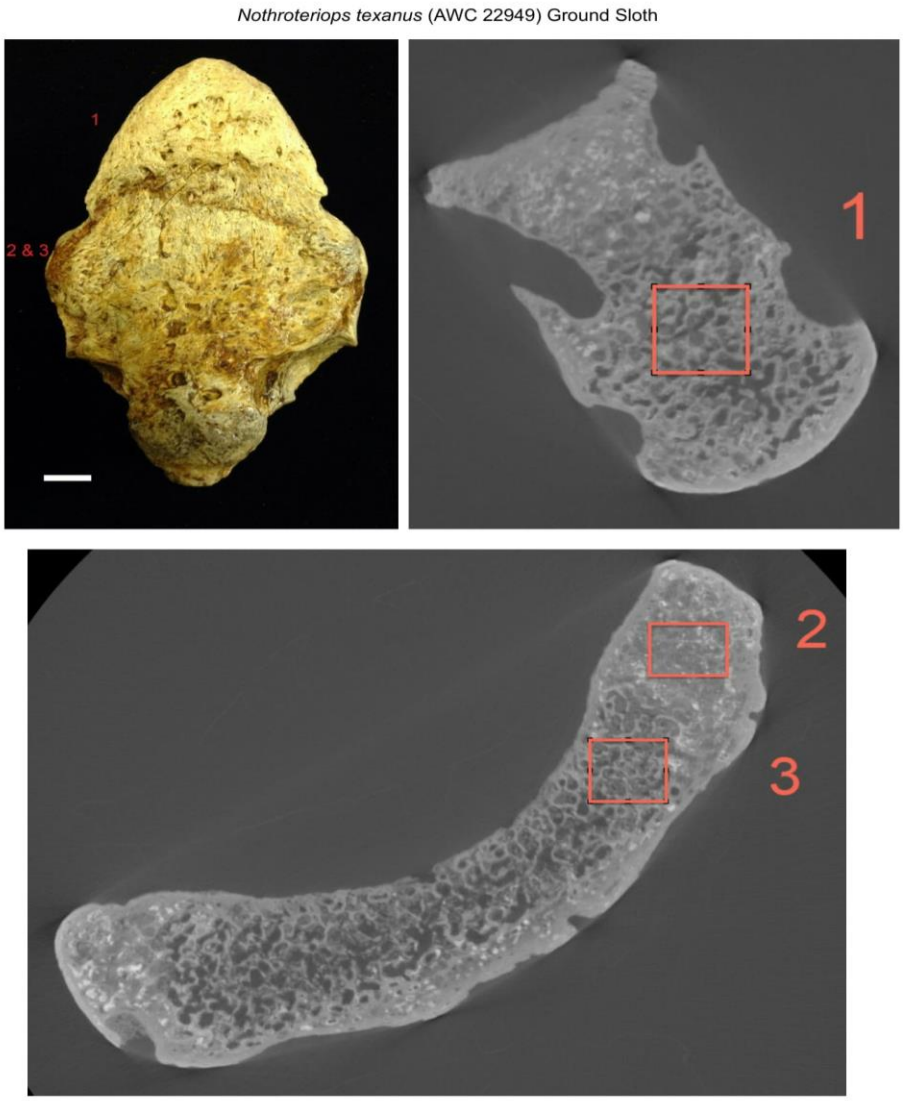

Figure 31. *Nothrotheriops texanus* species with an original photograph of the presternum (top left). Red numbers on the left of the full image correspond to the locations of the ROIs (red boxes) on the slices of the other two images generated in Fiji. Box 1, 2, and 3 correspond to mediocranial, lateral, and mediocaudal elements, respectively. Scale equals 10 mm.

Four species of the comparative dataset - *Cabassous tatouay, Eidolon dupreanum, Homo sapiens,* and *Gorilla gorilla gorilla* - were selected for further analysis. Effects of external forces were evaluated on the trabecular characteristics in central zones and were compared to zones that articulate with marginal structures (Fig. 32).

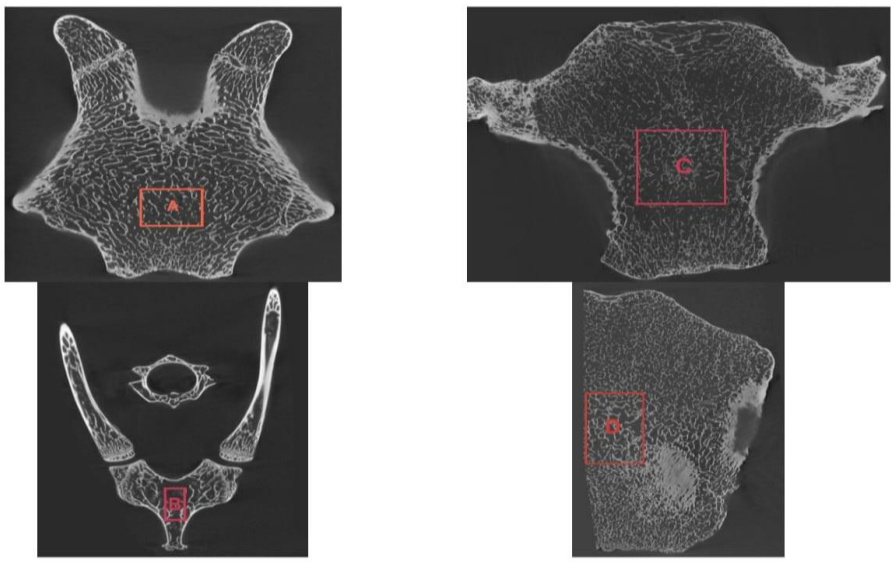

Species/Letter	Statistical Significance	Rose Diagram	Dom Dir	Coherency	%Bone
Cabassous tatouay /A	A vs all p<0.001 B vs all p<0.001 C vs all p<0.001 D vs all p<0.001		-71.48	0.28	17
Eidolon dupreanum / B			-82.20	0.18	10
Homo sapiens / C			76.27	0.12	17
Gorilla gorilla gorilla / D			-76.63	0.08	26

Figure 32. For each species the top panel shows pictures of the micro CT scan slice with a red square put around the central zone for analysis in Fiji. The bottom panel shows trabecular orientation data of each ROI. The second column gives the results of a statistical comparison using the Watson Wheeler non-parametric test between the current central zone and all of the corresponding ROIs from Fig. 30. The third column shows rose diagrams created using R. For this circular representation of the data, the values between 0 and 179 degrees were were replicated between 180 and 359 degrees. The fourth, fifth and sixth columns show parameters for Dominant Direction (Dom Dir) in degrees, Coherency and % ratio of bone to total area (% Bone) for each ROI, respectively. Scale size in all equals 5 mm except for *Gorilla* and *Homo*, where it equals 10 mm.

Two adjacent ROIs within the same presternal element were selected for evaluating the significance in difference of trabecular orientations in *Cabassous tatouay* (Fig. 33). The same species also shows the most overt and extreme boundaries on the surface of the presternum. Micro CT scans reveal that this holds true within the presternum as well (Fig. 34). Boundaries and trabecular orientations across the boundaries were analyzed for significance in orientation and evaluated in the Discussion (data from Fig. 30, *Cabassous tatouay,* ROI 1 vs ROI 2).

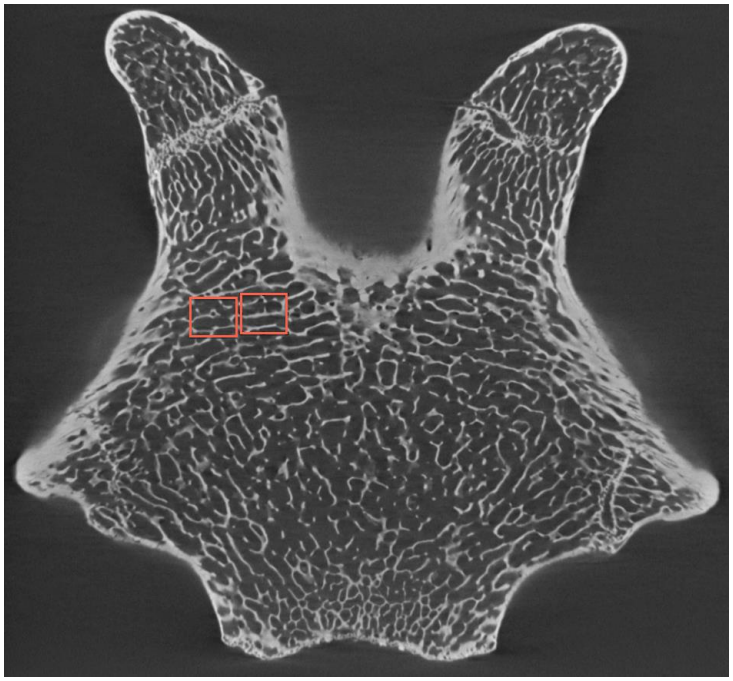

ROI	Statistical Significance	Rose Diagram	Dom Dir	Coherency	%Bone
Left	Left vs Right p<0.001	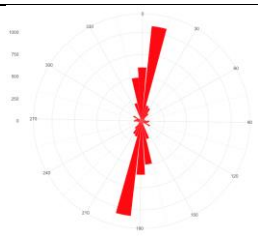	4.53	0.35	20.1
Right		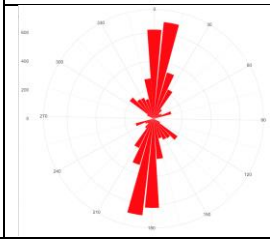	6.94	0.45	23.6

Figure 33. The top panel shows a picture of the micro CT scan of *Cabassous tatouay* with red squares put around two adjacent slices from the same lateral zone. The bottom panel shows trabecular orientation data of each ROI. The third column shows rose diagrams created using R.

For this circular representation of the data, the values between 0 and 179 degrees were were replicated between 180 and 359 degrees. The fourth, fifth and sixth columns show parameters for Dominant Direction (Dom Dir) in degrees, Coherency and % ratio of bone to total area (% ratio) for each ROI, respectively.

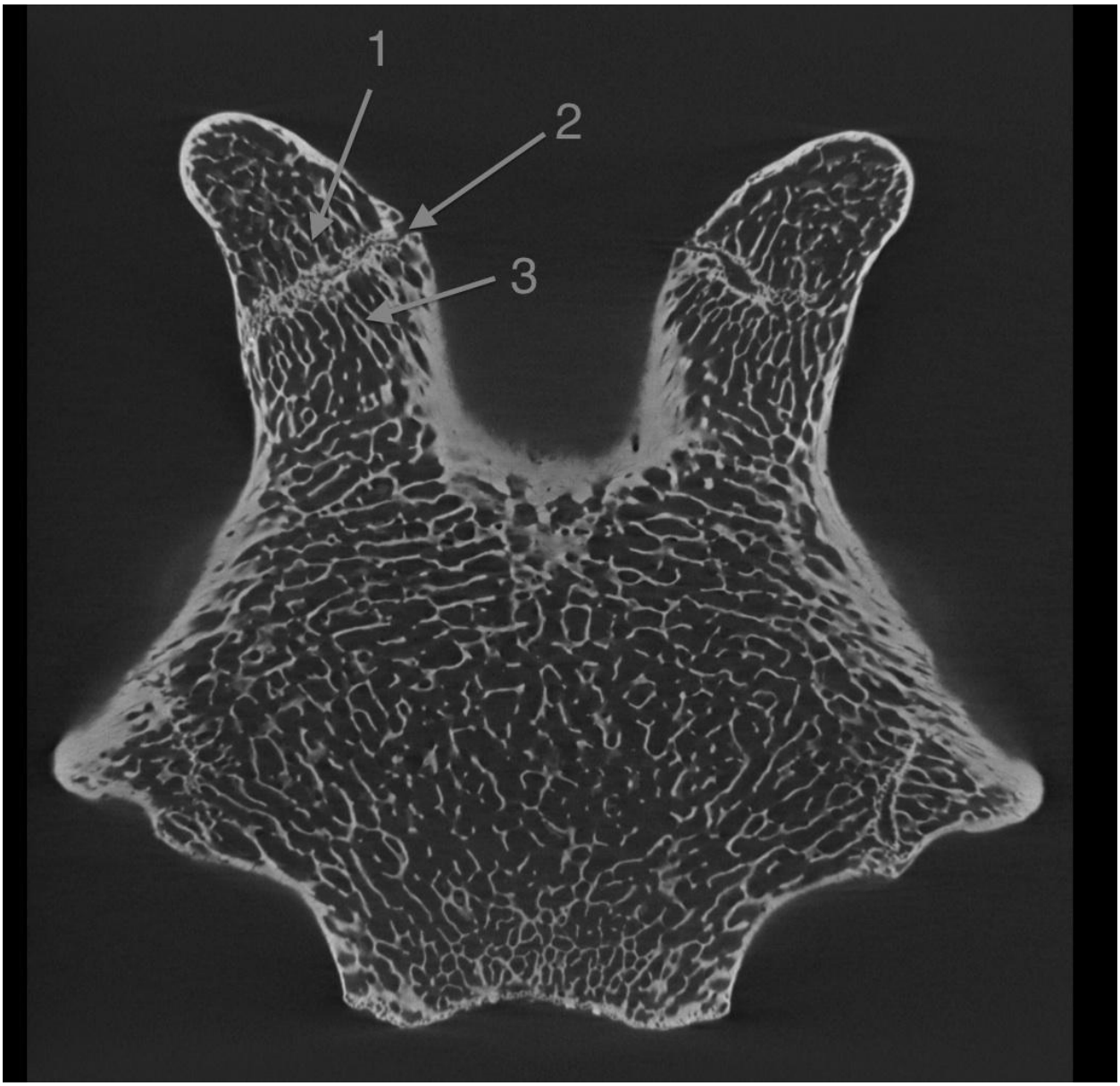

Figure 34. Arrows pointing at the boundary (arrow 2) and trabecular orientations across the boundary (arrows 1 and 3) of *Cabassous tatouay.*

4. Discussion

The diversity of sternal structure across the mammalian radiation has resulted in multiple controversial interpretations of its evolutionary transformation. In contrast to the sternum of ancestral synapsids and cynodonts, the sternum of eutherian mammals is smaller in both relative size and in count of elements. This reduction is most marked in the presternum, which is a single element in living eutherians. Current theories variably suggest that the reduction in presternal element count is a result of evolutionary loss, element fusion, or both (Klima, 1973, 1985, 1987; Luo 2007, 2011, 2015). In this project, the positional, structural, and ontogenic framework of the presternum was examined to evaluate these hypotheses. The project used anatomical imaging of thoracic scans of an ontogenetic series of humans, and adult scans of comparative fossil and living taxa. Key observations of the project, and their implications, are discussed below.

4.1. Multiple eutherian taxa possess composite presterna. The eutherian presternum is classically described as a single element that articulates anteriorly with the clavicle, laterally with the first thoracic rib, and posteriorly with both the second thoracic rib and the first sternebrae. In 2017, Feldman documented the presence of multiple elements in the presternum of several adult ground sloth *Paramylodon harlani* individuals, suggesting that it may instead be composite (Fig. 12). A key result of this project was documentation of the existence of a composite presternum in *Homo sapiens*. Of the 346 human individuals surveyed from the Weaver medical thoracic CT scans, 10.7% exhibit more than one presternal element. This is strong evidence for the existence of multiple presternal elements in humans, as was previously observed by Bayarogullari et al. (2012). It also suggests that element fusion occurs during ontogeny, because all individuals above the age of 10 exhibit a single presternal unit (Fig. 24 and Table 3).

The lack of defined presternal elements in adult humans suggested that further evidence for composite sterna might be limited to early developmental stages and/or basal mammalian taxa. Because only adult specimens were available, comparative taxa were chosen from basal taxa and/or those with extreme adaptations. Overt boundaries of presternal elements were found in five of the ten taxa surveyed - *Tamandua tetradactyla* (Pilosa, MCZ 34961), *Nothrotheriops texanus* (Pilosa, MCZ 22949), *Dasypus bellus* (Cingulata, UF 224700), *Cabassous tatouay* (Cingulata, MCZ 1021), and *Eidolon dupreanum* (Chiroptera, MCZ 45068) (Fig. 30). Composite presterna have previously been reported in manatees and dugongs (Sirenia, Buchholtz et al. 2014) and in cetaceans (Buchholtz, unpub.). This suggests that a composite presternum is widely distributed among eutherian taxa, even if rarely recognizable in adults.

4.2. Progressive fusion of elements is characteristic. Another key observation is that progressive sternal fusion is widespread: it occurs within all component parts - presternum, mesosternum, and xiphisternum - of the human sternum during ontogeny. Fusion between the presternum and mesosternum is evident in the later decades of life as seen in individual W564 (Fig. 28, individual 8), between the mesosternum and xiphisternum (Fig. 29), and between the presternum and the first ribs (Fig. 28, individuals 5 - 9). In addition to fusion of the major

structural units, the presternal elements also show an ontogenetic progression of fusion. The data reported here convincingly demonstrate that there is a reduction in the count of presternal elements with age (Fig. 24, Table 3). Additionally, scans of three individuals taken in close succession to each other, i.e. a few months to a few years apart (Figs. 25-27), reveal that developmentally expansion of the presternum occurs. Especially individual W622, which belongs to pattern H, has a segmented presternum that hints the fusion of the lateral and mediocaudal elements towards the major structure (Fig. 27). Although not conclusive, this suggests that initially separated presternal elements fuse during ontogeny.

4.3. Conserved number and positional relationships of presternal elements. Feldman (2017) recognized three presternal elements in the fossil ground sloth *Paramylodon harlani* and identified them as mediocranial, mediocaudal and lateral (Fig. 11 and Fig.12). Both the lateral and the medial caudal elements are paired, the mediocranial element lies in the midline and is unpaired (Fig. 12). Presternal elements similar in number and position occur across taxa, which strongly suggests that this ancestral presternal composition has been inherited from a common ancestor. Although these presternal elements are expressed variably in different taxa, the components are positionally conserved (Fig. 30).

4.4. Element identifications can be proposed from location and articular contacts. A key challenge of this project was to propose the evolutionary homologs of presternal elements. The identity of the mediocranial unit is unambiguous. Early synapsids (e.g. *Dimetrodon*, Fig. 3) have a single median ventral sternal element - the interclavicle - that articulates with the clavicles. Cynodonts (e.g. *Diademodon,* Fig. 4) and living monotremes (e.g. *Tachyglossus*, *Ornithorhynchus*, Fig. 5) also exhibit a single, unpaired, medial sternal element that articulates with the clavicles. This element also articulates posteriorly with a bilateral element usually called the “manubrium”. These observations suggest that the mediocranial unit is the homolog of the interclavicle, and is the ancestral base to which other, later, components fuse. Like the interclavicle of model mammals, it is almost certainly of neural crest origin (Rodriguez-Vazquez et al., 2012).

In contrast to the interclavicle, the mediocaudal unit is a paired structure. It lies immediately anterior the sternebrae of the mesosternum, and like them it is separated from adjacent sternebra(e) at locations where it articulates with ribs. The lateral plate mesoderm origin of the sternal bands is well-established across many mammalian taxa (e.g. Burke and Nowicki, 2003). Developmentally, the somitic ribs initially inhibit hypertrophy of the lateral plate mesoderm sternal bands at their sites of interaction, initiating a secondary, axially-influenced “segmentation” of an originally continuous structure (Chen, 1952). Such inhibition is expected in these tissues with different mesodermal origins. Location, development, and articulation all argue that the mediocaudal element is the anteriormost subdivision of the sternal bands.

The two paired lateral elements lie at the lateral margin of sides of the presternum and are separated by the mediocaudal elements. This element has not been previously recognized in fossil or living mammals. In fact, a separate lateral element is not known in the adult of any adult mammal skeleton except the ground sloth *Paramylodon harlani* (Feldman 2017).

Nevertheless, we find it in all of the taxa in this project that exhibit composite sterna. Each lateral element articulates with the first rib on its respective side. This articulation is distinctive because although it is the site of interaction between lateral plate mesoderm and somitic cells, in this case the tissues of different origin do not have an inhibitory interaction, but fuse. Because it lies at the contact zone of structures from two different developmental domains, it may act to mediate their interaction. The work of Durland et al. (2008) suggests that at least the ventral portion of the first rib (and only the first rib) has been repatterned as an abaxial tissue. It seems likely therefore that the first rib : lateral presternal element is an abaxial : abaxial interaction. If so the lateral element would play a role analogous to that of the tiny sacral ribs, which fuse on one side to the somitic primaxial vertebrae and on the other to the LPM abaxial ilium in the mammalian pelvis (Griffin and Angielczyk, 2019) and also show abaxial patterning (Durland et al. 2008) despite their somitic origin. The homolog of the lateral element of the presternum is unknown.

4.5. Variable ontogenetic sequence and timing of element fusion. The pattern of element fusion is variable in the Weaver database of human individuals (Figs. 16-22). Even in the youngest age group, there are individuals with a single presternal unit, which by inference is the result of early element fusion. When multiple elements are present, they occur in several different patterns, indicating variable patterns of fusion. Individuals with separation of either one of the lateral elements (Figs. 18, 20, 21, or patterns D, F, H), both of the lateral elements (Fig. 22, or pattern I), one of the mediocaudal elements (Figs. 19, 21, or patterns E, H), or both of the mediocaudal elements (Figs 17, 20, 22, or patterns B, F, I) were identified. Both average age and age range was generated for each pattern (Table 2 and Fig. 23, respectively). The correspondence between the increase in age and the decrease in the number of segmented elements is striking (Fig. 24, Table 3). These observations further support the inference of the ontogenetic fusion of elements.

However, interpretation of the timing of the sequence of fusion is difficult. In early synapsids and monotremes we can infer that the lateral elements have already fused with the mediocaudal element (sternal bands) because the first thoracic rib articulates with this “manubrium,” and because the mediocranial element remains as a separate unit (Fig. 4-5). These taxa can even be classified as belonging to pattern C (Fig. 15), which we did not observe in humans. In humans that sequence of fusion can be interpreted as variable. In addition, the timing of fusion during ontogeny is also broadly variable (Fig. 23). For example, following the fusion of the lateral element, which was recognized to its articulation with the first rib: individual W849, aged 0.72, belonging to pattern I, had its lateral element located more posterior, closer to the mediocaudal element (Fig. 22). But, individual W681, age 0.33, belonging to pattern F, had its lateral element located more anterior, closer to the mediocranial element (Fig. 20). This observation suggests that there is no well-defined pattern and timing of fusion of the presternal elements, and particularly of the lateral element, during ontogeny.

4.6. Trabecular histology does not support variation in presternal elements based on developmental origin. The recognition of multiple taxa with composite presterna raised the question of whether presternal elements, known to have different developmental origins, have

different histological signatures. Analysis at micro CT scan level was conducted to examine presternal element histology (Fig. 30). Even though trabecular orientation patterns vary within a single presternum, the boundaries that separate trabecular patterns do not appear to coincide with the boundaries between developmental units. For example, in *Cabassous tatouay,* trabeculae with a predominant orientation in the mediocranial element maintain their orientation across the boundary into the mediocaudal unit (Fig. 34). Similarly, more than one trabecular orientation frequently occurs within a single developmental unit. For example, the mediocaudal unit of *Cabassous tatouay* has regions of trabeculae with more than one predominant orientation (Fig. 30, *Cabassous tatouay* Box 4 vs Box 6 vs Fig. 32, Box A). Analogous patterns exist for the factors of coherency and percent bone.

In apparent contrast to these trends, the evaluation of trabecular structure using the OrientationJ plug-in of Fiji showed statistical differences in trabecular orientation distribution between every pair of ROIs within every individual. This was true for the analysis of 180 one-degree bins or for the analysis of 18 consolidated ten-degree bins. These results are treated here with skepticism, because analysis of adjacent ROIs in a single element within an individual also yield statistically significant differences in trabecular orientation, despite apparent similarity in dominant direction and coherency (Fig. 33). Again, the very large number of computer-generated observations for each ROI (see Materials&Methods) allowed for a very fine-grained analysis of angular orientation. Even though the predominant direction of two ROIs can be identical or very similar, the distribution of all observation in the ROI could still be statistically unique because of variations far outside the dominant direction of the trabeculae (see histograms in Fig. 30). For our purposes dominant directionality and coherency seem more appropriate measures and can be easily interpreted from the Rose diagrams.

These measures and patterns indicate the role of other factors. These other factors are most likely a form of continuous bone remodeling that is an adaptive response to the mechanical forces involved (Kivell, 2016). Adaptive remodelling is clearest in animals with extreme adaptations. A comparison of the presternal structures in mammals with different uses of their forelimbs due to differences in lifestyle supports this preliminary hypothesis.

There is an apparent high bone density, higher coherency and a dominant direction of trabeculae oriented at high angles to presternal boundaries at the locations adjacent to articulating structures. In contrast, areas that do not directly interact with adjacent articulating structures have a lower coherency and bone density. In our dataset these trends were most vividly illustrated by *Cabassous tatouay* (Fig. 30, *Cabassous tatouay* and Fig. 32, Box A). For example, at the central zone, where there are presumably no direct tensive mechanical forces, little preference for orientation with a high isotropy was shown (Fig. 31, Box A). Compared to the marginal ROIs as in Fig. 30, the central area showed lower coherency and lower bone ratio (Fig. 32). Another extreme example in our dataset was *Eidolon dupreanum* (Fig. 30, *Eidolon dupreanum* and Fig. 32, Box B). The central zone showed minimal to no trabeculae, which resulted in no preferred orientation, a low coherency and a low percent bone, compared to the marginal ROIs in Fig. 30 (Fig. 32, Box B). In contrast, *Homo sapiens* and *Gorilla gorilla gorilla* showed almost no change in coherency of dominant orientation of trabeculae and percent

bone between middle and marginal zones (Fig. 30, *Homo sapiens* and *Gorilla gorilla gorilla*, Fig. 32 Box C and Box D). These observations strongly suggest that trabecular orientation, coherency, and bone density reflect the functional adaptation of trabeculae. Animals that are bipedal such as *Homo sapiens* and *Gorilla gorilla gorilla* have a very modest differentiation between zones. Animals with an extreme use of the forelimb such as the burrower *Cabassous tatouay* and the flier *Eidolon dupreanum* show a greater differentiation between zones. Although the results are preliminary they suggest that the histological analysis of the presternum may be able to predict the functional adaptation of animal. But any trabecular patterns are not unique to developmental origin.

Bone remodeling of the appendicular skeleton due to strain has been most often studied in appendicular bones such as the humerus and/or femur (reviewed by Kivell, 2016). For example, Fajardo and Muller (2001) investigated trabecular changes of micro CT scans of the humerus and femur in different primate species. Those with an arboreal lifestyle had more isotropic trabeculae compared to terrestrial primates that have a more general use of their shoulders and hips (Fajardo and Muller, 2001). A similar trend within the species used in this project was observed. Those with a lifestyle that demands preferred and repetitive use of the forelimb such as burrowers and active fliers also have a preferred trabecular orientation with a high coherency at the marginal ends located adjacent to articulating structures. In contrast, bipedal mammals with a less intense and more diffuse usage of muscles attaching to the presternum show a broader distribution of orientations and coherency values that approach isotropy. Differential trabecular structure in the presternum is therefore a possible new tool for interpreting limb use and lifestyle in taxa when limb analysis is not possible or non-informative.

4.7. The term “manubrium” is not appropriate for referencing the presternum. In early synapsids and monotremes, the presternal structure posterior to the interclavicle is referred to as a “manubrium” (Figs. 4 and 5), whereas in eutherians the whole presternum, including the fused interclavicle, is considered to be the “manubrium” (Fig. 6). This interchangeable use of the term “manubrium” is ambiguous. Firstly, the interclavicle has a different developmental origin. It is recognized as a separate element in synapsids and monotremes and as a fused element in eutherians. Based on these reference mammalian groups, the same term is used when referring to developmentally and functionally different elements of the presternum. The mediocaudal elements are serial anterior homologs of the sternebrae of the mesosternum. They articulate with the posterior sternebrae and the second rib in the same way as subsequent sternebrae and ribs do. Often, the paired sternal bands alone are referred to as the “manubrium”. However, in this project the presence of another developmental element - the paired lateral element - was documented. The lateral elements are the only presternal, or even sternal, structure that fuses directly with a rib. This suggests that the lateral element may mediate the integration of the somitic first rib to the LPM sternum across the lateral somitic frontier. Because the term “manubrium” is variable and contradictory, it should be abandoned. Rather, the more precise reference to each element should be used when being specific, and the term presternum should be used when being general.

5. Conclusions

This project agrees with Klima (1973, 1985, 1987) and Luo (2007, 2011, 2015) that there has been a reduction in the count of elements in the mammalian presternum over evolutionary time. In contrast to Luo and Klima, however, it suggests that reduction has been the product exclusively of fusion and not of loss. It confirms the initial observations of Feldman (2017) of the presence of a previously unrecognized presternal element, here called the lateral presternal element. Further, it documents its presence and fusion sequence during ontogeny of the human sternum.

The project proposes that despite fusion during ontogeny, the articulations of each of the original presternal elements has been retained. It seems likely that this retention reflects the demands of unique interactions and marginal articulations of these developmentally disparate elements. These histories and articulating elements serve as the basis for proposing element homologies.

No unique histological signature of individual elements was found. Rather, trabecular orientation appears to reflect limb use and muscle attachment. Continuity of trabecular structure across element boundaries suggests full ontogenetic integration and common osteogenic response to mechanical stressors. The variable morphology of the presternum in living mammals is further hypothesized to exhibit adaptive remodeling in response to a wide variety of lifestyles.

Finally, the use of the term “manubrium” in reference to parts of the presternum is suggested to be abandoned. Instead, original element references should be used.

Each of the project’s major findings demand further exploration. These should include the analysis of *Nothrotheriops texanus* with a more powerful computer, the extension of the functional studies to a broader range of comparative taxa with more diverse lifestyles, and the location of potential datasets that would allow the observation of fusion in other ontogenetic series.

6. Literature Cited

Angielczyk, K. 2009. *Dimetrodon* Is Not a Dinosaur: Using Tree Thinking to Understand the Ancient Relatives of Mammals and their Evolution. *Evo Edu Outreach.* 2: 257-271.

Arbabi, A. 2009. A quantitative analysis of the structure of human sternum. *J Med Phys.* 34: 80-86.

Barchilon, V., Hershkovitz, I., Rothschild, B., Wish-Baratz, S., Latimer, B., Jellema, L., Hallel, T., Arensburg, B. 1996. Factors affecting the rate and pattern of the first costal cartilage ossification. *Am J Forensic Med Pathol.* 17: 239-47.

Bayaroğulları, H., Yengil, E., Davran, R., Ağlagül, E., Karazincir, S., Balcı A. 2014. Evaluation of the postnatal development of the sternum and sternal variations using multidetector CT. *Diagn Interv Radiol.* 20: 82–89.

Buchholtz, E., Wayrynen K., and Lin, I. 2014. Breaking constraint: axial patterning in Trichechus (Mammalian: Sirenia). *Evolution & Development* 16: 382-303.

Burke, A., and Nowicki, J. 2003. A new view of patterning domains in the vertebrate mesoderm. *Developmental Cell.* 4: 159-165.

Chen, J. 1952. Studies on the morphogenesis of the mouse sternum. *J Anat.* 86: 373–401.

Darwin, C. 1859. On the Origin of Species by Means of Natural Selection, or Preservation of Favoured Races in the Struggle for Life. John Murray, London.

Durland, J., Sferlazzo, M., Logan, M., Burke, A. 2008. Visualizing the lateral somitic frontier in the Prx1Cre transgenic mouse. *J Anat.* 212: 590-602.

Doube, M., Kłosowski, M., Arganda-Carreras, I., et al. 2010. BoneJ: Free and extensible bone image analysis in ImageJ. *Bone*. 47: 1076–1079.

Fajardo, R., Muller, R. 2001. Three-dimensional analysis of non-human primate trabecular architecture using micro-computed tomography. *Am J Phys Anthropol.* 115: 327-336.

Feldman, A. 2017. Is the mammalian presternum composite: Evidence from *Paramylodon harlani*. Unpublished BISC 350 thesis, Wellesley College.

Gaetano, L., Mocke, H., & Abdala, F. 2018. The postcranial anatomy of *Diademodon tetragonus* (Cynodontia, Cynognathia). *Journal of Vertebrate Paleontology*. 38, e1451872.

Griffin, C. and Angielczyk, K. 2019. The evolution of the dicynodont sacrum: constraint and innovation in the synapsid axial column. *Paleobiology.* 45: 201-220.

Griffiths, M. 1978. The Biology of the Monotremes. Academic Press, New York.

Hunt A. P. and Lucas S. G. 2005. Permian Fossil Vertebrates from the Panhandle of Texas, USA, pp. 115 - 117 *in* S. G. Lucas and K.E. Ziegler, eds., The Nonmarine Permian. New Mexico Museum of Natural History and Science, Bulletin 30.

Keibel F. and Mall FP. 1912. *Manual of Human Embryology II.* J. B. Lippincott Company, Philadelphia.

Keyte, A. and Smith, K. 2010. Developmental origins of precocial forelimbs in marsupial neonates. *Development.* 137: 4283-4294.

Klima, M. 1973. Die Fruhentwicklung des Schultergurtels und des Brustbeins bei den Monotremen (Mammalia: Prototheria). *Advances in Anatomy, Embryology & Cell Biology.* 47: 1-80.

Klima, M. 1985. Development of shoulder girdle and sternum in mammals. *Fortschritte der Zoologie.* 30: 81-94.

Klima, M. 1987. Early development of the shoulder girdle and sternum in marsupials (Mammalia: Metatheria). *Advances in Anatomy, Embryology & Cell Biology.* 109: 1-91.

Kivell, T. 2016. A review of trabecular bone functional adaptation: what have we learned from trabecular analyses in extant hominoids and what can we apply to fossils? *J. Anat.* 228: 569-594.

Luo, Z.-X. 2007. Transformation and diversification in the early mammalian evolution. *Nature* 450: 1011-1019.

Luo, Z., Yuan, C., Meng, Q., and Ji., Q. 2011. A Jurassic eutherian mammal and the divergence of marsupials and placentals. *Nature* 476: 442-445.

Luo, Z. 2015. Origin of the mammalian shoulder girdle, pp. 167-187 *in* Great Transformations in Vertebrate Evolution. University of Chicago Press, Chicago.

Müller, F. and O'Rahilly, R. 1986. Somitic-vertebral correlation and vertebral levels in the human embryo. *Am J Anat.* 177: 3-19.

Oftadeh, R., Perez-Viloria, M., Villa-Camacho, J. C., Vaziri, A., & Nazarian, A. 2015. Biomechanics and mechanobiology of trabecular bone: a review. *Journal of Biomechanical Engineering.* 137: 0108021–01080215.

Owen, R. 1846. Report on the Archetype and Homologies of the Vertebrate Skeleton. Report of the British Association for the Advancement of Science (Southampton Meeting), pages 169-340.

Parker, W. 1868. A monograph on the structure and development of the shoulder-girdle and sternum in the Vertebrata. The Ray Society, London.

Raff, R. 1996. The Shape of Life. University of Chicago Press, Chicago.

Rezakhaniha, R., Agianniotis, A., Schrauwen, J., Griffa, A., Sage, D., Bouten, C., N. van de Vosse, F., Unser, M., Stergiopulos, N. 2012 Experimental investigation of collagen waviness and orientation in the arterial adventitia using confocal laser scanning microscopy. *Biomech Model Mechanobiol*. 11: 461–473.

Riedl, R. 1978. Order in Living Organisms: A Systems Analysis of Evolution. John Wiley & Sons, Chichester.

Rodríguez-Vázquez, J. F., Verdugo-López, S. , Garrido, J. M., Murakami, G. and Kim, J. H. 2013. Morphogenesis of the manubrium of sternum in human embryos: A New Concept. *Anat Rec*, 296: 279-289.

Romer, A. 1927. The pelvic musculature of ornithischian dinosaurs. *Acta Zool.,* 8: 225-275.

Romer, A. 1956. The Vertebrate Body. W. B. Saunders Company, Philadelphia.

Ruge, G. 1880. Untersuchungen uber Entwicklungsvorgange am Brustbein und an der Sterno-clavicularverbindung des Menschen. *Gegenbaurs Morph Jahrb.* 6: 362 - 414.

Sereno, P. C. 2006. Shoulder girdle and forelimb in a Cretaceous multituberculate: Form, functional evolution, and a proposal for basal mammalian taxonomy; Chpt. 10, pp. 315-370 in M. T. Carrano, T. J. Gaudin, R. W. Blob, and J. R. Wible (eds.), Amniote Paleobiology: Perspectives on the Evolution of Mammals, Birds, and Reptiles. University of Chicago Press, Chicago.

Struthers, J. 1889. Memoir on the Anatomy of the Humpback Whale, *Megaptera longimana*. Maclachlan and Stewart, Edinburgh.

Valasek, P., Theis, S., DeLaurier, A., Hinits, Y., Graham N. Lukea, Otto, A., Minchin, J.,
He, L., Christ, B., Brooks, G., Sang, H., Evans, D., Logan, M., Huang, R., Patel, K. 2011. Cellular and molecular investigations into the development of the pectoral girdle. *Developmental Biology* 357: 108-116.

Wagner, G. 1994. Homology and the Mechanisms of Development, pp. 274-299 in Homology: The Hierarchical Basis of Comparative Biology, B. K. Hall, ed. Academic Press, San Diego.

7. Acknowledgements

I could not have completed this thesis without my mentor **Emily Buchholtz**. Thank you for letting me peek at the phenomenal fingerprints evolution and physiology leave on anatomy. Thank you for your endless encouragement, bottomless patience, priceless moments of joy and excitement and most importantly for your light and guidance! I am privileged to have you as my first mentor in academic research. A debt of gratitude also goes to my thesis committee members, who have been a source of limitless support and enlightenment – **Kim O'Donnell, John Cameron,** and **Kenneth Hawes**. Your teaching and devotion to your students is how I aspire to be in the future when I get a chance to. And thank you **Wellesley College** for your internal support.

This project would not have been possible without **Aisling Farrell**, Collections Manager La Brea Tar Pits and Museum for the loan of the *Paramylodon harlani* specimens; **Dr. Amy Sato**, Veterinary Radiologist at the Tufts University Cummings School of Veterinary Medicine, for the scanning of the *Paramylodon harlani* specimen; **Mark Omura**, Collections Manager, Mammalogy, Harvard University Museum of Comparative Zoology, for the loan of comparative living specimens; **Richard C. Hulbert**, Collections Manager, Division of Vertebrate Paleontology Florida Museum of Natural History, for the loan of the *Dasypus bellus* specimen; **Dr. Fred Croxen**, Professor of Geosciences, Arizona Western College, for the loan of the *Nothrotheriops texanus* specimen; **Dr. Zhexi Luo**, Department of Organismal Biology and Anatomy, University of Chicago, for the CT dataset of the *Tachyglossus* specimen; **H. Greg McDonald**, Bureau of Land Management and **Tim Gaudin**, University of Tennessee, Department of Geosciences for museum identification and photography of the *Paramylodon harlani* specimens at the La Brea Tar Pits Museum. Additionally, thank you **Aaron Nakasone** for being kind, for sharing insights on image analysis In ImageJ and BoneJ, and for scanning the comparative specimens. Thank you to **Dr. Ashley Weaver** of Wake Forest University Medical School for letting us use your patients' dataset of human CT scans. Thank you, **Asher Feldman ('17)** for being the inspiration to continue this project that began in 2017.

Thank you to my amazing **friends** and supportive **family friends**, you were all so important throughout this process. Thank you for valuing what I do and for giving me refreshing perspective maybe not on the thesis, in particular, but on life, in general.

To **my family**. Not once did you stop supporting me. Your intelligence and persistence never stop inspiring me. You paved the way for me and I walk it by your example. Thank you for cheering me up and reminding me why I do what I do.